

# An emerging global aerosol climatology from the MODIS satellite sensors.

Lorraine A. Remer<sup>1</sup>, Richard G. Kleidman<sup>1,2</sup>, Robert C. Levy<sup>1,2</sup>, Yoram J. Kaufman<sup>1,9</sup>, Didier Tanré<sup>3</sup>, Shana Mattoe<sup>1,2</sup>, J. Vanderlei Martins<sup>1,4</sup>, Charles Ichoku<sup>1,5</sup>, Ilan Koren<sup>6</sup>, Hongbin Yu<sup>1,7</sup>, and Brent N. Holben<sup>8</sup>

## Popular Summary

The aerosol product derived from MODIS observations now includes a seven year record from Terra-MODIS and a five year record from Aqua-MODIS. We are now at a point to use this information in the manner intended, to perform a quantitative “check-up” of Earth’s global aerosol system. How are aerosols distributed over the continents and oceans? How are different sizes distributed, and what are the relationships between aerosol loading and aerosol particle size in different regimes? Finally, what are the regional and seasonal characteristics of the aerosols? In this paper we will attempt to answer these questions from the data base of MODIS aerosol products.

We first evaluate the latest version of the MODIS data product and find that the retrieval of aerosol over land is substantially better than previous versions, and the ocean retrieval about the same. However, a bias has been introduced between Terra and Aqua retrievals that was not present in previous collections of MODIS aerosol data. This bias is significant, and not yet understood. Despite this unexplained bias, we do understand the MODIS retrievals well enough to describe the aerosol system as seen from space over the past 5 to 7 years.

- Global mean AOD is 0.13 over ocean and 0.19 over land
- Land shows a broader distribution of AOD than ocean. Roughly 28% of land retrievals are extremely clean and within  $\pm 0.05$  of AOD = 0. Only 15% of ocean retrievals are that low.
- Global mean values are limited by sampling issues. No retrievals are made during polar night, snow, ice or bright land surfaces.

- Global mean values can vary by as much as 20% depending on how the data is aggregated, weighted and averaged. The results here are “pixel weighted”. Thus, they are biased to clear skies and the reported AOD may be low.
- AOD in situations with 80% cloud fraction are twice the global mean values, although such situations occur only 2% of the time over ocean and less than 1% of the time over land.
- There is no drastic change in aerosol particle size associated with these very cloudy situations.
- The heaviest aerosol regions are North Africa, India, East and Southeast Asia. Each has its own seasonal cycle and interannual variability.
- The northern industrial economies (North America and Europe), Siberia and especially Australia have the lowest AODs.
- The three southern hemisphere biomass burning regions (South America, southern Africa and Indonesia) exhibit very similar seasonal behavior.
- Taken as a whole there is an increasing trend in southern hemisphere biomass burning AOD over the five year Aqua record.
- We find that elevated aerosol over background conditions in most oceanic regions is dominated by fine mode aerosol and not dust. This includes the Mediterranean, the north Pacific downwind of Asia and even the southern oceans. Only the Saharan outflow region in the Atlantic and the Arabian Sea area have certain months dominated by dust.
- In this analysis we did not find significant global trends of AOD either over land or ocean. A longer time series is required to identify trends.

# An emerging global aerosol climatology from the MODIS satellite sensors.

Lorraine A. Remer<sup>1</sup>, Richard G. Kleidman<sup>1,2</sup>, Robert C. Levy<sup>1,2</sup>, Yoram J. Kaufman<sup>1,9</sup>, Didier Tanre<sup>3</sup>, Shana Mattoo<sup>1,2</sup>, J. Vanderlei Martins<sup>1,4</sup>, Charles Ichoku<sup>1,5</sup>, Ilan Koren<sup>6</sup>, Hongbin Yu<sup>1,7</sup>, and Brent N. Holben<sup>8</sup>

## Abstract

The recently released Collection 5 MODIS aerosol products provide a consistent record of the Earth's aerosol system. Comparison with ground-based AERONET observations of aerosol optical depth (AOD) we find that Collection 5 MODIS aerosol products estimate AOD to within expected accuracy more than 60% of the time over ocean and more than 72% of the time over land. This is similar to previous results for ocean, and better than the previous results for land. However, the new Collection introduces a 0.015 offset between the Terra and Aqua global mean AOD over ocean, where none existed previously. Aqua conforms to previous values and expectations while Terra is high. The cause of the offset is unknown, but changes to calibration are a possible explanation. We focus the climatological analysis on the better understood Aqua retrievals. We find that global mean AOD at 550 nm over oceans is 0.13 and over land 0.19. AOD in situations with 80% cloud fraction are twice the global mean values, although such situations occur only 2% of the time over ocean and less than 1% of the time over land. There is no drastic change in aerosol particle size associated with these very cloudy situations. Regionally, aerosol amounts vary from polluted areas such as East Asia and India, to the cleanest regions such as Australia and the northern continents. In almost all oceans fine mode aerosol dominates over dust, except in the tropical Atlantic downwind of the Sahara and in some months the Arabian Sea.

1 An emerging global aerosol climatology from the MODIS  
2 satellite sensors.

3  
4 Lorraine A. Remer<sup>1</sup>, Richard G. Kleidman<sup>1,2</sup>, Robert C. Levy<sup>1,2</sup>, Yoram J. Kaufman<sup>1,9</sup>,  
5 Didier Tanré<sup>3</sup>, Shana Mattoe<sup>1,2</sup>, J. Vanderlei Martins<sup>1,4</sup>, Charles Ichoku<sup>1,5</sup>, Ilan Koren<sup>6</sup>,  
6 Hongbin Yu<sup>1,7</sup>, and Brent N. Holben<sup>8</sup>

7  
8  
9     1 Laboratory for Atmospheres, NASA Goddard Space Flight Center, Greenbelt MD  
10    2 Science Systems and Applications, Inc., Lanham MD  
11    3 Laboratoire d'Optique, Atmosphérique, Villeneuve d'Ascq, France  
12    4 Department of Physics, University of Maryland Baltimore County  
13    5 Earth System Science Interdisciplinary Center, University of Maryland, College  
14      Park  
15    6 Weizman Institute, Rehovot Israel  
16    7 Goddard Earth Science and Technology Institute, University of Maryland  
17      Baltimore County  
18    8 Laboratory for Terrestrial Physics, NASA Goddard Space Flight Center,  
19      Greenbelt MD  
20    9 Deceased

21  
22  
23  
24         Submitted to *Journal of Geophysical Research – Atmospheres*

25         *The Yoram J. Kaufman Symposium on Aerosols, Clouds and Climate*

26                     November 30, 2007

27  
28  
29         Corresponding author:

30     Lorraine A. Remer  
31     Laboratory for Atmospheres, Code 613.2  
32     NASA/Goddard Space Flight Center  
33     Greenbelt MD 20771  
34     301-614-6194  
35     301-614-6307 (fax)  
36     Lorraine.A.Remer@nasa.gov

37

37   **Abstract**

38

39   The recently released Collection 5 MODIS aerosol products provide a consistent record  
40   of the Earth's aerosol system. Comparison with ground-based AERONET observations  
41   of aerosol optical depth (AOD) we find that Collection 5 MODIS aerosol products  
42   estimate AOD to within expected accuracy more than 60% of the time over ocean and  
43   more than 72% of the time over land. This is similar to previous results for ocean, and  
44   better than the previous results for land. However, the new Collection introduces a 0.015  
45   offset between the Terra and Aqua global mean AOD over ocean, where none existed  
46   previously. Aqua conforms to previous values and expectations while Terra is high. The  
47   cause of the offset is unknown, but changes to calibration are a possible explanation. We  
48   focus the climatological analysis on the better understood Aqua retrievals. We find that  
49   global mean AOD at 550 nm over oceans is 0.13 and over land 0.19. AOD in situations  
50   with 80% cloud fraction are twice the global mean values, although such situations occur  
51   only 2% of the time over ocean and less than 1% of the time over land. There is no  
52   drastic change in aerosol particle size associated with these very cloudy situations.  
53   Regionally, aerosol amounts vary from polluted areas such as East Asia and India, to the  
54   cleanest regions such as Australia and the northern continents. In almost all oceans fine  
55   mode aerosol dominates over dust, except in the tropical Atlantic downwind of the  
56   Sahara and in some months the Arabian Sea.

57

58   **Introduction**

59

60   The instruments aboard NASA's Terra and Aqua satellites have been observing the Earth  
61   since early 2000 and mid-2002, respectively. In the words of Dr. Yoram J. Kaufman,  
62   Terra Project Scientist at the time of the Terra launch, the Terra and Aqua missions were  
63   “designed for a comprehensive check-up of planet Earth” [Kaufman, 2000  
64   <http://terra.nasa.gov/Events/FirstImages/>]. Similar to a check-up at the doctor’s office,  
65   these missions would characterize the health of the planet. The goal was to use the  
66   vantage point of space to view the Earth’s interconnected systems of atmosphere, land

67 and ocean, and to characterize the parameters important to sustainability of the planet and  
68 its human population.

69

70 One important feature measured by several instruments aboard Terra and Aqua is  
71 atmospheric aerosol. These small solid or liquid particles suspended in the atmosphere  
72 play a major role in the energy balance of the Earth, in modifying cloud, precipitation,  
73 and atmospheric circulation characteristics, in providing nutrients to nutrient-limited  
74 regions of land and oceans, and in affecting air quality and public health. Aerosols are  
75 highly inhomogeneous in space, time and composition, and yet, knowing the amount,  
76 composition, distribution, size and shape of these particles is necessary for any  
77 meaningful estimates of their effect, from estimating anthropogenic climate forcing to  
78 forecasting air quality and potential health effects from air pollution.

79

80 One of the instruments aboard both Terra and Aqua specifically designed to characterize  
81 atmospheric aerosols is the MODerate resolution Imaging Spectroradiometer (MODIS).  
82 The aerosol product derived from MODIS observations now includes a seven year record  
83 from Terra-MODIS and a five year record from Aqua-MODIS. We are now at a point to  
84 use this information in the manner intended, to perform a quantitative “check-up” of  
85 Earth’s global aerosol system. How are aerosols distributed over the continents and  
86 oceans? How are different sizes distributed, and what are the relationships between  
87 aerosol loading and aerosol particle size in different regimes? Finally, what are the  
88 regional and seasonal characteristics of the aerosols? In this paper we will attempt to  
89 answer these questions from the data base of MODIS aerosol products.

90

## 91 **MODIS aerosol products**

92

93 The aerosol products are derived operationally from spectral radiances measured by  
94 MODIS. MODIS has 36 channels spanning the spectral range from 0.41 to 15  $\mu\text{m}$   
95 representing three spatial resolutions: 250 m (2 channels), 500 m (5 channels), and 1 km  
96 (29 channels). The aerosol retrieval makes use of seven of these channels (0.47 – 2.13  
97  $\mu\text{m}$ ) to retrieve aerosol characteristics [Remer et al., 2005] and uses additional

98 wavelengths in other parts of the spectrum to identify and mask out clouds and river  
99 sediments [Ackerman et al., 1998, Gao et al., 2002; Martins et al., 2002; Li et al., 2003].  
100 The MODIS aerosol algorithm is actually two independent algorithms, one derives  
101 aerosol characteristics over land and the other for aerosols over ocean. The original land  
102 algorithm is based on the “dark target” approach [Kaufman and Sende 1988; Kaufman et  
103 al., 1997; Remer et al., 2005] and therefore does not retrieve over bright surfaces  
104 including snow, ice and deserts. A more recent MODIS product, labeled “Deep Blue”  
105 does retrieve over bright surfaces [Hsu et al., 2004]. However, the climatology presented  
106 in this paper does not include the “Deep Blue” results. The ocean algorithm masks out  
107 river sediments, clouds and sunglint, then inverts the radiance at 6 wavelengths (0.55 -  
108 2.13  $\mu\text{m}$ ) to retrieve aerosol optical depth (AOD) and particle size information [Tanré et  
109 al., 1996; 1997].

110  
111 We will examine two types of aerosol products: aerosol optical depth (AOD) and particle  
112 size parameter. AOD is a straightforward measure of column integrated extinction. The  
113 MODIS product includes retrievals of AOD at seven wavelengths over ocean and three  
114 wavelengths over land. There are several measures of particle size included in the  
115 MODIS aerosol product. Angstrom exponent over land is defined as:

116

$$117 \quad \text{AngExp} = -\frac{\ln(AOD470/AOD660)}{\ln(470/660)}$$

118

119 There are two Angstrom exponents over ocean, defined as

120

$$121 \quad \text{AngExp1} = -\frac{\ln(AOD550/AOD870)}{\ln(550/870)}$$

122

123 and

124

$$125 \quad \text{AngExp2} = -\frac{\ln(AOD870/AOD2130)}{\ln(870/2130)}$$

126

127 Angstrom exponent is a measure of the spectral dependence of the aerosol optical depth  
128 and a proxy for aerosol size. Larger Angstrom exponents indicate smaller particles,  
129 while smaller Angstrom exponents suggest larger particles.

130

131 There are two other measures of particle size in the MODIS aerosol product, and these  
132 are fine aerosol optical depth and fine mode/model fraction. Fine AOD is the AOD  
133 contributed by the fine mode aerosol model. Over ocean, the fine model is a single mode  
134 with effective radius spanning the range 0.10 to 0.25  $\mu\text{m}$  [Tanré et al., 1997]. These are  
135 mostly submicron particles, but the tail of the mode could include particles that exceed 1  
136  $\mu\text{m}$ . Likewise, there could be submicron particles associated with the tail of the coarse  
137 mode distribution that are not included in the Fine AOD. Over land, the “fine” model is a  
138 multi-modal aerosol model that includes both fine and coarse modes [Levy et al., 2007a].  
139 It is labeled a “fine” model because the fine mode dominates the size distribution.

140 Therefore, fine AOD has entirely different meanings whether over ocean or land. Fine  
141 mode/model fraction is the fine AOD divided by the total AOD. We use fine “mode” to  
142 designate the parameter over ocean because the model is a single mode, and fine “model”  
143 to designate the multi-modal model over land, but abbreviate both as FMF.

144

145 The derived aerosol products undergo rigorous testing and validation. The algorithms  
146 were created before Terra launch and tested using data from airborne imagers [Kaufman  
147 et al., 1997; Tanré et al. 1997, 1999; Chu et al., 1998]. After Terra launch, the products  
148 were validated by comparison with collocated ground-based observations by the Aerosol  
149 Robotics NETwork (AERONET). The AERONET network consists of hundreds of  
150 automatic instruments that measure aerosol optical depth (AOD) to within 0.01 accuracy  
151 [Holben et al., 1998; Eck et al. 1999; Smirnov et al., 2000], and retrieve other aerosol  
152 characteristics including particle size information [Dubovik and King, 2000; O’Neill et  
153 al., 2003]. Comparison of MODIS-derived AOD with collocated AERONET-measured  
154 data showed that the MODIS AOD ocean products were accurate to within  $\pm 0.03 \pm 0.05 \tau$   
155 over ocean, where  $\tau$  is AOD [Ichoku et al, 2002; Remer et al., 2002; Levy et al., 2003,  
156 2005; Remer et al., 2005}. Additional validation using the NASA Ames Airborne  
157 Tracking Sunphotometer confirmed these error bounds over ocean [Russell et al. 2007;

158 Livingston et al., 2003; Redemann et al., 2005, 2006]. Over land, the comparison yielded  
159 varying results. In some cases the over land AOD retrievals fell within expected  
160 uncertainties ( $\pm 0.05 \pm 0.15\tau$ ) [Chu et al., 2002; Ichoku et al., 2002; Remer et al., 2005],  
161 but in many situations there appeared to be a strong positive bias at low AOT in the over  
162 land retrieval, and a negative bias at high AOT [Ichoku et al., 2003, 2005; Levy et al.,  
163 2005; Remer et al., 2005]. The MODIS particle size information over ocean correlated  
164 well with AERONET retrievals, but tended to over predict the occurrence of small  
165 particles at the expense of large particles [Kleidman et al., 2005].

166

167 To address these lingering problems with the aerosol products, new codes were  
168 developed. The land algorithm underwent significant change, while maintaining the  
169 basic dark target approach [Levy et al. 2007ab]. The ocean algorithm remained almost  
170 the same with changes made only to three of the nine aerosol models in the Look Up  
171 Table [Remer et al., 2007]. These new algorithms were applied operationally to the  
172 complete record of calibrated radiances to generate a new “Collection” of aerosol  
173 products resulted. These reprocessed data are known as Collection 5, which is available  
174 for both the Terra and Aqua records. Collection 5 provides us with a consistent data set  
175 created from a single set of algorithms applied identically to an uninterrupted data stream  
176 of calibrated radiances. Collection 5 aerosol products exist for both Terra and Aqua  
177 records.

178

179

180

## 181 **Data for the Climatology**

182

183 Two types of MODIS data will be used in this paper: Level 2 (L2) and Level 3 (L3).  
184 MODIS L2 aerosol data are ungridded 10 km retrievals of various aerosol parameters  
185 available at the time of satellite overpass. These data represent the fundamental MODIS  
186 aerosol product. The product consists of geophysical parameters such as aerosol optical  
187 depth and aerosol particle size information, as well as a quality assurance (QA) flag that  
188 indicates the level of reliability of each retrieved pixel. QA flags range from 0 (lowest

189 quality) to 3 (highest quality). Comparison of the L2 data, collocated in time and location  
190 with high quality ground measurements provide the ‘validation’ of the basic product.

191

192 MODIS L3 data are an aggregation of the L2 data onto a gridded  $1^{\circ} \times 1^{\circ}$  global grid and  
193 represent the statistics including the mean and weighted means of the L2 product  
194 contained within the grid square. L3 data are available on a daily basis, as well as 8 day  
195 and monthly means. The global gridded data of L3 will provide the basic set of data for  
196 the climatology presented here.

197

198 Creating daily L3 from L2, and further processing the data to achieve global and regional  
199 monthly means requires decisions as to how to aggregate and average the data at each  
200 step. Depending on what processing is chosen variations in the final values can vary by  
201 as much as 20% [Levy et al., submitted]. In this work we start with high quality daily L3  
202 data, weight by the number of L2 retrievals in the 1 degree grid square (pixel-weighted)  
203 and calculate monthly means and other statistics. The reason for this decision is to  
204 minimize the contribution of retrievals in cloud fields, where artificially enhanced AOD  
205 occurs frequently. It is incongruous for the monthly mean of a particular grid square  
206 determined by just one 10 km retrieval on one day of the month to count equally with  
207 another grid square that consisted of hundreds of 10 km retrievals in that month. On the  
208 other hand, we want global representation of the data without contributions from QA=0  
209 data. Pixel-weighting the quality weighted product in this manner introduces some  
210 inconsistencies detailed in Levy et al. [submitted], and is not the same as making the  
211 same calculations directly from the 10 km L2 data.

212

### 213 **Comparison of Collection 5 Against AERONET Observations**

214

215 We evaluate the Collection 5 aerosol products by comparing with collocated AERONET  
216 observations. A preliminary evaluation was performed and reported in Levy et al.,  
217 [2007b] and Remer et al. [2007], but that evaluation was confined to a test bed of MODIS  
218 radiance granules. We note that while the test bed produced a substantial number of  
219 collocations, it was still limited in time and space. Furthermore, the test bed consisted of

220 saved Collection 4 radiances. When Collection 5 was processed, not only were the  
221 aerosol retrieval algorithms upgraded to Collection 5, but the basic calibration  
222 coefficients were changed as well. Thus, the radiances used to create Collection 5  
223 aerosols are different than those used for Collection 4. When we compare MODIS  
224 aerosol products to AERONET now, we evaluate simultaneously both the changes we  
225 made to the aerosol algorithms and the changes made to the calibration that affect the  
226 aerosol retrieval.

227

228 Figure 1 shows the results of collocating MODIS aerosol optical depth retrievals with  
229 AERONET for the ocean retrieval following the spatio-temporal technique of Ichoku et  
230 al. [2002]. Two wavelengths and both Terra and Aqua are shown. The ocean  
231 comparison is made for any island or coastal AERONET station within 25 km of the  
232 ocean. The only station eliminated from this analysis is Mauna Loa because of its high  
233 elevation in comparison to the ocean surface. Because the ocean retrieval quality flags  
234 are regarded as ‘conservative’ [Russell et al., 2007] we include data of all quality in the  
235 comparison. The plots show data that were sorted according to AERONET AOD,  
236 grouped into 25 bins of near equal samples and then mean and standard deviation were  
237 calculated. The regression equations plotted and correlation coefficients indicated were  
238 calculated from the full cloud of collocated points before binning and averaging. The  
239 data used in this plot spans the length of the mission from the beginning to the end of  
240 2006.

241

242 MODIS aerosol optical depth retrieved over ocean is strongly correlated to the  
243 corresponding AERONET values for both wavelengths and both satellites. Expected  
244 error for ocean retrievals is  $\pm 0.03 \pm 0.05\tau$ . AOD retrievals at the 870 nm channel fall  
245 within expected error more than 2/3 of the time. Retrieval results for shorter wavelengths  
246 are less consistently accurate, falling within expected error only 60% of the time at 550  
247 nm. These results for Collection 5 are similar to those reported for Collection 4 [Remer  
248 et al., 2005].

249

250 Figure 2 shows the results of comparing Collection 5 retrievals over land with  
251 AERONET AOD. Again these are “global” plots making use of all AERONET stations  
252 except COVE and Venise, which are both located on stand alone ocean platforms far  
253 from shore. Unlike the ocean validation exercise, for land we use those retrievals with  
254 the highest quality labels (QA = 3). Over land, the inclusion of lower quality retrievals  
255 will make significant difference in the validation plots, lowering the correlation and  
256 decreasing the percentage of retrievals within expected error. We recommend to users to  
257 check quality flags over land and to use caution when using retrievals with QA < 3.  
258 Similar numbers of collocations are available for both land and ocean despite the fact that  
259 there are many more AERONET stations over land than near ocean. The requirement on  
260 the land quality flag eliminates many collocations from the analysis. Thus, while there  
261 are more opportunities to compare with AERONET over land, there are fewer locations  
262 where a high quality land retrieval is possible. The plots in Figure 2 are prepared in the  
263 same manner as in Figure 1, although only one channel is shown.

264

265 MODIS aerosol optical depth over land in Collection 5 is a strong improvement of the  
266 results from Collection 4 [Remer et al., 2005]. More than 72% of retrievals fall within  
267 expected error over land at 550 nm. In Collection 4, 68% of retrievals fell within  
268 expected error at that wavelength. More importantly there was an overall positive mean  
269 bias in Collection 4 of +41%. In Collection 5 we see insignificant bias, with 0 mean bias  
270 in Terra and -7% bias in Aqua. Note that the expected error over land is greater than  
271 over ocean ( $\pm 0.05 \pm 0.15\tau$ ).

272

273 The comparison of AOD retrievals over land and ocean show that the Collection 5  
274 retrieval is producing results either as accurate as Collection 4 (ocean) or much improved  
275 (land), at least in a global sense. There appears to be little difference between Terra and  
276 Aqua. Validation efforts beyond the scope of this paper continue. Individual regions will  
277 be examined, and we will include ship board measurements as well as AERONET  
278 observations as the “ground truth”. However, for now, we see that the MODIS  
279 Collection 5 aerosol product can be used to examine the state of the aerosol system.  
280

281

282 **Comparison of Collection 5 with Collection 4**

283

284 By comparing MODIS retrieved AOD with collocated AERONET observations on a day  
285 by day basis we established that the Collection 5 retrievals are a true representation of the  
286 Earth's aerosol system, to within specified accuracies. Even if both Collection 5 and  
287 Collection 4 [Remer et al., 2005] aerosol optical depth match AERONET observations  
288 within MODIS specifications, there could still be systematic offsets. In this section we  
289 compare mean results of the two Collections.

290

291 Over ocean, the only difference between Collection 4 and Collection 5 aerosol algorithms  
292 is that three of the aerosol models were modified. The new aerosol optical models are  
293 given in Table 1. AERONET retrievals of aerosol optical properties available only after  
294 Terra-MODIS launch suggested that the real part of the refractive index for coarse mode  
295 sea salt particles was smaller than the 1.43 used in the original algorithm. Changing the  
296 three coarse mode 'sea salt' aerosol models in the algorithm to a real part refractive index  
297 of 1.35 in accordance with Dubovik et al., [2002 and personal communication] was tested  
298 by applying the new aerosol models to our test bed of saved Collection 4 radiances. The  
299 results are shown in Figure 3. The changed aerosol models reduced the positive bias in  
300 the fine mode fraction retrieved by Collection 4 [Kleidman et al., 2005], while not  
301 making any significant changes to the AOD retrieval. Both Aqua and Terra data were  
302 used during testing. The mean AOD using either software was 0.15, but the mean fine  
303 mode fraction changed from 0.47 to 0.39. Thus we did not expect any changes to the  
304 AOD from Collection 4 results, but did expect reduced fine mode fraction.

305

306 Figure 4 shows a comparison of monthly global mean AOD over oceans between  
307 Collection 4 and Collection 5, separated by satellites. Unlike Figure 3 the data used to  
308 create Figure 4 do not come from our saved test bed of radiances. These data, instead,  
309 come directly from the operational data base available to all users. The Collection 4  
310 AOD values were processed with Collection 4 radiances as input, while the Collection 5  
311 AOD values were processed with Collection 5 radiances as input. Note, that updates in

312 calibration cause Collection 5 radiances to differ from Collection 4. The data plotted  
313 include only the period of overlap of all four data sets, from August 2002 when Aqua  
314 began processing data to August 2005 when Collection 4 production ended. In Figure 4  
315 we see that for the Aqua satellite global mean AOD is basically the same for both  
316 Collections, as expected, but for Terra Collection 5 it is approximately 0.015 higher than  
317 Collection 4. Note that 0.015 is well within the expected uncertainty of  $\pm 0.03 \pm 0.05\tau$ .  
318 Further analysis shows that Terra Collection 4 matches both Aqua Collections and that  
319 Terra Collection 5 is an outlier when compared to the other three data sets.

320  
321 The 0.015 offset in AOD between Terra Collection 5 and the other three data sets is not  
322 yet understood. Algorithm changes were applied equally to the software run for Terra  
323 and Aqua. If an AOD offset was introduced by modifying the aerosol models as  
324 described above, then we would see AOD changes equally in both satellites. Because the  
325 offset has been introduced to Terra and not Aqua, we suspect this offset is due to updates  
326 to the Terra-MODIS calibration constants that altered the Collection 5 input radiances.  
327 Investigation continues. However, in this paper we will concentrate on Aqua retrievals  
328 over ocean, and leave the evaluation of Terra ocean retrievals until a time when the  
329 calibration changes to Terra have been carefully evaluated.

330  
331 Over land, in contrast to ocean, substantial differences exist between the Collection 4 and  
332 5 algorithms [Levy et al., 2007ab]. All aerosol optical models were modified, as were  
333 surface assumptions and snow masking. A vector radiative transfer code replaced the  
334 scalar code used in Collection 4, and the overall numerics of the inversion were changed.  
335 Because of these changes we expect Collection 5 to have substantially different AOD  
336 values than Collection 4, and they do. The changes made to the aerosol land algorithm  
337 resulted in the improved comparison plots against AERONET. (See Figure 2). Mean  
338 AOD over land has decreased from 0.28 in Collection 4 to 0.19 in Collection 5. Because  
339 of the drastic changes over land, subtle changes due to calibration changes will be lost in  
340 the analysis. For the purposes of this paper, to be consistent with the analysis over ocean,  
341 we will focus on the Aqua satellite. The land Collection 5 algorithm and comparison with

342 Collection 4 is satisfactorily documented in the recent papers Levy et al. [2007a] and  
343 [2007b], and will not be further discussed here.

344

345

346 **Global mean aerosol optical depth over ocean and land**

347

348 Proceeding with Aqua Collection 5 we will now investigate the emerging global aerosol  
349 climatology as viewed by MODIS. Figure 5 shows the time series of monthly and global  
350 mean AOD through the Aqua record. The data are separated by ocean and land  
351 retrievals. Over ocean the global mean AOD at 550 nm is 0.13, 10% of all ocean  
352 retrievals are below 0.041 and 10% are above 0.235. The mean ocean AOD is close to  
353 the 66<sup>th</sup> percentile value showing that the distribution is skewed towards lower values.  
354 There is no significant trend in the global mean ocean AOD over the five year Aqua  
355 record. There is a significant trend in the Terra record discussed in Remer et al.,  
356 [submitted]. The fine mode AOD, also plotted in Figure 5 follows the month by month  
357 variations of the total AOD. Mean fine mode AOD is approximately 0.06. Note that fine  
358 mode AOD contains fine mode contributions from marine aerosol and transported dust  
359 and pollution, and is thus not the same as the anthropogenic component.

360

361 Over land the global mean AOD at 550 nm is 0.19, 10% of all land retrievals are negative  
362 and 10% are above 0.44. Note that the land retrieval permits negative AOD retrievals in  
363 order to avoid positive bias in the large-scale statistics [Levy et al., 2007b]. The physical  
364 meaning of the negative values is that there is no difference between small negative  
365 values, zero AOD or small positive values. Approximately 20% of the AOD retrievals  
366 over land are essentially zero. Over ocean the retrieval has greater sensitivity to small  
367 values of AOD and thus there are fewer negative retrievals. The ocean retrieval 10<sup>th</sup>  
368 percentile already contains AOD values above the noise threshold. The mean land AOD  
369 is also close to the 66<sup>th</sup> percentile showing the same skewed distribution as over ocean.  
370 Similar to ocean, there is no significant trend in the global mean AOD over land in the  
371 five year Aqua record. The mean fine mode AOD is 0.10, which is larger than over  
372 ocean. Furthermore, over ocean we saw that fine mode AOD tracked with the total AOD

373 month by month. Peaks in total AOD corresponded to peaks in fine mode AOD. Over  
374 land total AOD peaks in early Spring, while fine mode AOD peaks in late Summer and  
375 Fall, where fine mode AOD can account for almost the total mean land AOD in that  
376 season. The seasonal cycles suggest a Spring maximum due to dust transport and a Fall  
377 maximum due to southern hemisphere biomass burning. However, there is a limit to the  
378 accuracy of the retrieval of aerosol size parameter over land. The fine mode AOD shown  
379 in the land plot of Figure 5 should be considered more of a qualitative indicator, rather  
380 than a validated quantitative product.

381

382 The statistics plotted in Figure 5 are calculated from pixel weighted QA-weighted L3  
383 daily data. Global mean values are strongly dependent on the way the data are  
384 aggregated, averaged and weighted. Resultant discrepancies in global mean values of  
385 20% are possible [Levy et al., submitted]. The pixel-weighted method used here will  
386 produce the lowest value of global mean AOD because it is biased to cloud free  
387 conditions. Aerosol retrievals in the vicinity of clouds can be contaminated by cloud 3D  
388 effects (Wen et al, 2006; 2007) and by subpixel clouds (Zhang et al, 2006). We chose  
389 this weighting method in order to minimize the effect of clouds on the statistics, although  
390 we acknowledge that pure aerosol in the vicinity of clouds can be higher than aerosol  
391 away from cloud fields (Koren et al., 2007). The consequence of our chosen method is  
392 that the values in Figure 5 may be biased low.

393

#### 394 **Global AOD statistics in the vicinity of clouds**

395

396 Figure 6 shows the global mean statistics calculated from the L3 daily data directly  
397 without first creating monthly means. The global mean AOD values calculated from the  
398 histograms are the same as those calculated from the monthly means of Figure 5. Evident  
399 are the same skewed nature of the AOD distributions, and the broader range and the  
400 negative values of the land histograms. In a global sense the fine mode fraction over  
401 ocean remains fairly constant over the range of ocean AOD values. Over land, however,  
402 the fine (model) fraction suggests that coarse aerosol dominates at low AOD,  
403 transitioning to more equal partitioning at moderate AOD. While this is physically

404 realistic over land, one should treat the results with skepticism, due to the large  
405 uncertainty of derived size parameter over land

406

407 The histogram analysis of Figure 6 permits examination of the effect of cloud fields on  
408 the aerosol statistics. The bottom panels of Figure 6 plot the AOD distributions for those  
409 grid squares in which the cloud fraction exceeds 80%. In these cloudy situations there is  
410 a drastic shift of AOD to higher values, both over ocean and land. The mean AOD for  
411 these cloudy situations more than doubles to 0.28 over ocean and to 0.44 over land. We  
412 expected this increase in AOD to be in part caused by cloud contamination. The aerosol  
413 retrieval would interpret large cloud droplets in the field of view as being coarse mode  
414 particles. If subpixel clouds and other contaminants were the cause of the drastic  
415 increase in AOD in cloudy situations we would expect a strong decrease in fine mode  
416 fraction. There is some decrease in fine mode fraction at moderate AOD over ocean, but  
417 not as much as would be expected from cloud contamination alone. Other factors  
418 including 3D effects and increase of AOD from increased humidity around clouds are  
419 also possible and would not decrease fine fraction in the same way as subpixel cloud  
420 contamination. Such factors could help to explain the increase of AOD in the cloudy  
421 situations without decreasing fine mode fraction. Note that these cloudy situations  
422 represent only 2% of the total number of grid squares included in the overall statistics  
423 over ocean and less than 1% over land.

424

## 425 **Regional and seasonal distribution of aerosol optical depth**

426

427 Up to this point we have analyzed the global aerosol system in terms of its global mean  
428 statistics. The aerosol system is far from being well mixed and homogenous. The  
429 aerosol story is very much linked to geography and season. Figure 7 shows four months  
430 of aerosol optical depth observed from Aqua MODIS. The four months were chosen to  
431 represent seasonal changes, and each month is the mean of that month over the five years  
432 of the Aqua mission. In Figure 7 we see the strong aerosol loading over eastern China,  
433 the Indo-Gangetic Plain of India and in the eastern tropical north Atlantic during all  
434 seasons. We see the aerosol from biomass burning in Africa begin in January north of

435 the equator and shift southward during the course of the year until it is joined by tropical  
436 biomass burning in the Amazon and Indonesia during northern Autumn. There is wide  
437 spread elevated AOD over the oceans during the Spring of each hemisphere, April in the  
438 north and October in the south. During northern Summer the Arabian Sea and India  
439 exhibit unusually high AOD values, while North America, Europe and northern Asia  
440 have their highest, though moderate, aerosol loading during the same season.

441

442 Figure 7 also shows the limits of the MODIS aerosol products to represent the global  
443 aerosol system. Large expanses of the globe are left blank during various seasons due to  
444 polar night or surfaces unsuitable for making a dark-target retrieval. The new Deep Blue  
445 product will fill in some of these spaces when combined with the standard aerosol  
446 products although that prospect is outside the scope of this study. Because of these  
447 missing regions, the global mean aerosol values described here may not be truly  
448 representative of the entire globe, particularly over land.

449

450

### 451 **Aerosol optical depth of individual regions**

452

453 We define 13 regions over ocean (following Remer and Kaufman 2006) and 14 regions  
454 over land to examine MODIS-derived aerosol characteristics in greater detail. Figure 8  
455 defines these regions. Seasonal and annual mean AOD are given for each region and  
456 season in Table 2 for ocean regions and Table 3 for land. The heaviest aerosol loading  
457 can be found over India and the surrounding oceans during northern summer (JJA). East  
458 Asia also exhibits heavy aerosol loading, but during northern spring (MAM). The  
459 southern tropical Pacific shows the lowest AOD, but MODIS-observed AOD over the  
460 Australian continent is even lower, although the Australian values fall within the land  
461 algorithm's noise level.

462

463 Because the seasonal cycle is most pronounced near the aerosol source regions over land  
464 we concentrate our seasonal analysis on the land regions. Figure 9 shows the AOD time  
465 series for four categories of regions: northern industrial economies, southern biomass

466 burning regions, dust dominated and Asia. The four regions grouped as northern  
467 industrial economies are west and east North America, north Europe and the  
468 Mediterranean Basin. These four regions track together exhibiting increased AOD in the  
469 Spring and Summer, but increasing to only moderate levels as compared to other regions  
470 of the globe. The Fall and Winter seasons have very low AOD with eastern North  
471 America surprisingly showing the lowest values of AOD during the winter. The  
472 Mediterranean region, which includes parts of North Africa and the Middle East as well  
473 as southern Europe has a longer aerosol season with higher AOD values both in summer  
474 and in winter than the other three regions.

475

476 The three southern biomass burning regions, South America, southern Africa and  
477 Indonesia, show very similar seasonal patterns, despite their widely varying locations.  
478 The biomass burning season in the southern hemisphere occurs during southern Spring  
479 (SON) on all three continents. There is a high degree of interannual variability in the  
480 AOD values at each location with an overall increasing trend when all three locations are  
481 taken as a whole. The AOD during the biomass burning season is roughly twice the  
482 AOD values of the northern industrial economies, excluding the Mediterranean.  
483 However, during the  $\frac{3}{4}$  of the year with no burning, South America and southern Africa  
484 have low AOD comparable with values in North America and northern Europe.

485

486 Northern Africa and India, grouped together because both are affected by dust  
487 transported from the Sahara and Arabia, have overall higher AOD than any of the  
488 previous regions. North Africa exhibits an irregular seasonal cycle with the highest  
489 values reported in later winter (February and March) at the peak of the northern  
490 hemisphere biomass burning season, but also a secondary seasonal peak that varies but  
491 generally appears in late summer when dust is dominant. India's seasonal cycle is more  
492 regular with a single longer aerosol season. AOD begins building in the spring and  
493 extends into early summer. A small regular secondary peak also occurs late in the year.  
494 In 2006, this secondary peak was larger than in previous years.

495

496 The fourth grouping of regions in Figure 9 are the Asian regions, excluding India and  
497 Indonesia, which were previously discussed. The Asian regions include Siberia, East  
498 Asia, which is mainly China, and Southeast Asia. The AOD values in Siberia are low,  
499 especially in autumn and winter. However, snow covers much of the region in winter  
500 and therefore, MODIS does not sample much of this region in that season. Summer  
501 AOD values in Siberia are comparable to summer values in North America and northern  
502 Europe. Note that Siberia seems to track with the Asian regions to the south, although at  
503 much lower aerosol loading. This suggests some commonality in aerosol transport or  
504 similarity of sources. East Asia and Southeast Asia track together showing an extended  
505 aerosol season that spans the spring and summer seasons. The AOD during the aerosol  
506 season shows interannual variability for both regions, but can exceed values from the dust  
507 regions of northern Africa, India or the southern hemisphere biomass burning regions.  
508 AOD values remain moderately high even for the autumn and winter months.

509

## 510 **Aerosol size characteristics of individual regions**

511

512 Aerosol particle size can be described by a variety of parameters in the MODIS aerosol  
513 data product including fine mode AOD, fine mode fraction and various Angstrom  
514 Exponents. These parameters provide subtle differences, but are more or less correlated  
515 with each other. The ocean algorithm uses 6 wavelengths and benefits from a fairly  
516 homogenous background surface. Therefore, the ocean product contains inherently  
517 greater information content than the land product, which uses only three wavelengths and  
518 is sensitive to the assumptions made about the spectral surface reflectance. In short, the  
519 size parameters from the ocean algorithm are more reliable than the land. Despite this  
520 fact, in the global analysis we showed global statistics of aerosol size parameter over land  
521 (which we took as a qualitative parameter) because random errors introduced in various  
522 regions may be reduced by global averaging. We are already aware of specific regions  
523 where the land size parameter is systematically wrong [Jethva et al., 2007] and prefer to  
524 wait until full characterization of the land size parameter is available before calculating  
525 regional climatological statistics. In the regional analysis we focus the size parameter  
526 analysis solely on the ocean retrievals.

527

528 Table 2 shows the seasonal and annual mean fine mode fraction (FMF) for the 13 ocean  
529 regions. Values range from 0.28 – 0.35 in pristine southern hemisphere regions to 0.60 –  
530 0.65 in the northern midlatitudes. These seasonal mean numbers conform to our  
531 expectations that pristine oceanic regions would be dominated by sea salt, a coarse mode  
532 aerosol, and therefore have smaller FMF, while northern midlatitudes would have a  
533 greater fine mode contribution from aerosol transported from land sources.

534

535 We obtain greater physical interpretation by plotting monthly mean aerosol size  
536 parameter against monthly mean total AOD, following Kaufman et al., [2005]. Figure 10  
537 shows the results for five regions. The results fall into two classes. Regions 2, 4, and 13  
538 fall into the first class. In this situation as aerosol optical depth is added to a baseline  
539 background value AOD of the fine mode increases as well. The slope of the regression is  
540 approximately 0.7 – 0.8. Region 6 represents the second class. Here AOD fine also  
541 increases as total AOD increases, but at a much slower rate. The slope of the class 2  
542 regression is approximately 0.3. We interpret these two classes as the difference between  
543 adding smoke/pollution to a background marine aerosol in which the slope is the higher  
544 value, and adding dust, which results in the smaller slope.

545

546 We expect elevated AOD in Region 2 to be pollution from North America and Europe.  
547 Likewise we expect elevated AOD in Region 6 to be dust from the Sahara. However, it  
548 is somewhat surprising that the elevated aerosol in Region 13 follows the  
549 smoke/pollution curve so tightly. This suggests that elevated aerosol in the southern  
550 circumpolar ocean has a strong biomass burning component, and indeed the seasonal  
551 means in Table 2 shows that elevated AOD and FMF occur during the southern  
552 hemisphere biomass burning season. We also expected that some of the elevated aerosol  
553 in Region 4 would have a dust component from transported Asian dust. Instead we see a  
554 tight correlation following the smoke/pollution curve. Figure 10 also plots Region 7, the  
555 northern Indian Ocean. Region 7 splits its monthly means to follow both curves. This  
556 suggests that in some months the aerosol is dust and other months it is smoke/pollution.

557

558 Table 4 gives several annual mean aerosol size parameters, and the regression slope and  
559 correlation coefficients following Figure 10 for each ocean region. Note that Region 7,  
560 which contains both classes from Figure 10 has a small slope, but a relatively low  $R^2$   
561 value. A low  $R^2$  gives indication that the region follows neither class. In some cases this  
562 is because some months follow the smoke/pollution curve and other months the dust  
563 curve (Regions 3 and 7), but in other cases the region remains pristine through all months  
564 and there is no elevated aerosol (Region 9).

565

566

566

567

568

569

570

571 **Discussion and Conclusions**

572

573 The MODIS aerosol product derived from 7 years of Terra data and 5 years of Aqua data  
574 has recently undergone reprocessing using a new algorithm labeled Collection 5.

575 Collection 5 represents both new aerosol software and new calibration coefficients,  
576 applied consistently through the entire data records of each MODIS sensor. Comparison  
577 of Collection 5 MODIS aerosol optical depth (AOD) retrievals over ocean and land with  
578 high quality AERONET observations shows agreement as good as Collection 4 for ocean  
579 and much improved for land. In fact, in Collection 5 the land algorithm is performing as  
580 well as the ocean algorithm, with similar or smaller offsets, regression slopes close to 1.0  
581 and similar or better correlation. Comparison with collocated AERONET products  
582 requires both MODIS and AERONET to report cloud free conditions. Situations where  
583 MODIS retrieves but AERONET does not will not be included in the analysis.

584 Validation efforts continue, and a more comprehensive validation study is in preparation.

585

586 The differences we expected to find between Collection 4 and Collection 5 included a  
587 shift to larger particle sizes over ocean but no change to ocean AOD. In the Aqua record,  
588 indeed that is exactly what we find. However, something else has occurred in the Terra  
589 record. Not only did the particle size shift in Terra ocean, but the global ocean AOD  
590 increased by 0.015. The MODIS aerosol software is applied equally to Terra and Aqua.  
591 To have Terra oceanic AOD shift by 0.015, while Aqua AOD remain the same is  
592 impossible. The only logical answer is that MODIS calibration constants also changed  
593 between Collections. This change in Terra calibration is under investigation. In the  
594 meantime, we have focused on the Aqua record because the results are as expected. It is  
595 possible that Terra's new calibration will prove to be the more accurate and the results  
596 shown here are artificially low.

597

598 We have presented an analysis of Aqua-MODIS aerosol optical depth and particle size  
599 information, over ocean and land, globally and regionally. We have shown time series  
600 and histograms. From this analysis we conclude:

601

- 602 - Global mean AOD is 0.13 over ocean and 0.19 over land
- 603 - At every decision point in the processing we have taken the road leading to lower  
604 values of global mean AOD. In particular by pixel weighting and using Aqua  
605 instead of Terra, the global mean AOD is lower by 0.015 to 0.04 than if calculated  
606 without pixel weighting and by using Terra.
- 607 - We feel that the higher range of values that would be achieved without pixel  
608 weighting contain cloud artifacts. Therefore we decided to produce values that  
609 are least affected by clouds and are at the lower range of the envelope.
- 610 - Land shows a broader distribution of AOD than ocean. Roughly 28% of land  
611 retrievals are extremely clean and within  $\pm 0.05$  of AOD = 0. Only 15% of ocean  
612 retrievals are that low.
- 613 - Global mean values are limited by sampling issues. No retrievals are made during  
614 polar night, snow, ice or bright land surfaces.
- 615 - Global mean values can vary by as much as 20% depending on how the data is  
616 aggregated, weighted and averaged. The results here are “pixel weighted”. Thus,  
617 they are biased to clear skies and the reported AOD may be low.
- 618 - AOD in situations with 80% cloud fraction are twice the global mean values,  
619 although such situations occur only 2% of the time over ocean and less than 1%  
620 of the time over land.
- 621 - There is no drastic change in aerosol particle size associated with these very  
622 cloudy situations.
- 623 - The heaviest aerosol regions are North Africa, India, East and Southeast Asia.  
624 Each has its own seasonal cycle and interannual variability.
- 625 - The northern industrial economies (North America and Europe), Siberia and  
626 especially Australia have the lowest AODs.

627 - The three southern hemisphere biomass burning regions (South America, southern  
628 Africa and Indonesia) exhibit very similar seasonal behavior.  
629 - Taken as a whole there is an increasing trend in southern hemisphere biomass  
630 burning AOD over the five year Aqua record.  
631 - We find that elevated aerosol over background conditions in most oceanic regions  
632 is dominated by fine mode aerosol and not dust. This includes the Mediterranean,  
633 the north Pacific downwind of Asia and even the southern oceans. Only the  
634 Saharan outflow region in the Atlantic and the Arabian Sea area have certain  
635 months dominated by dust.  
636 - In this analysis we did not find significant global trends of AOD either over land  
637 or ocean. A longer time series is required to identify trends.

638

639 We demonstrate in this work an emerging climatology of aerosol characteristics using the  
640 satellite view from MODIS. Longer records are necessary to fully characterize trends  
641 and further analysis with multiple data sets is necessary to better unravel the signatures of  
642 aerosols and clouds. However, this view from space and “check-up” of the aerosol  
643 system provides valuable information for understanding the planet now and estimating  
644 the potential consequences of global change.

645

#### 646 **Acknowledgements**

647

648 This work was first put in motion almost three years ago by our co-author, mentor and  
649 dear friend, Yoram Kaufman. He actively participated in designing several figures and in  
650 organizing the latter half of the paper. Since then, not only did tragedy take him from us,  
651 but the MODIS reprocessing to Collection 5 required a revisit to the original analysis and  
652 a discussion of new validation. We only hope that the paper in present form does justice  
653 to his original vision. We miss Yoram’s guidance and inspiration almost every single  
654 day. We also wish to acknowledge the many AERONET PIs and their site managers who  
655 make the AERONET program possible. The research was supported by NASA’s  
656 Radiation Sciences Program and Earth Observation System Project Office.

657

658    **References**

659

660 Ackerman, S.A., K.I. Strabala, W.P. Menzel, R.A. Frey, C.C. Moeller and L.E. Gumley,  
661 1998: Discriminating clear sky from clouds with MODIS. *J. Geophys. Res.*, **103**, 32139-  
662 32140.

663

664 Chu, D. A., Y. J. Kaufman, L. Remer, and B. N. Holben, 1998: Remote sensing of  
665 smoke from MODIS Airborne Simulator during the SCAR-B Experiment. *J. Geophys.  
666 Res.* (special issue on SCAR-B), **103**, 31979-31987.

667

668 Chu, D. A., Y. J. Kaufman, C. Ichoku, L. A. Remer, D. Tanre, and B. N. Holben, 2002:  
669 Validation of MODIS aerosol optical depth retrieval over land. *Geophys. Res. Lett.*, **29**,  
670 doi: 10.1029/2001GL013205.

671

672 Dubovik, O. and M. D. King, 2000: A flexible inversion algorithm for retrieval of  
673 aerosol optical properties from Sun and sky radiance measurements," *J. Geophys. Res.*,  
674 **105**, 20 673-20 696.

675

676 Eck, T.F., B.N.Holben, J.S.Reid, O.Dubovik, A.Smirnov, N.T.O'Neill, I.Slutsker, and  
677 S.Kinne, 1999: Wavelength dependence of the optical depth of biomass burning, urban  
678 and desert dust aerosols, *J. Geophys. Res.*, **104**, 31 333-31 350.

679

680 Gao, B.-C., Y.J. Kaufman, D. Tanré and R.-R. Li, 2002: Distinguishing tropospheric  
681 aerosols from thin cirrus clouds for improved aerosol retrievals using the ratio of 1.38-  
682  $\mu\text{m}$  and 1.24- $\mu\text{m}$  channels. *Geophys. Res. Lett.*, **29**, 1890, doi:10.1029/2002GL015475.

683

684 Holben, B.N., T.F. Eck, I. Slutsker, D. Tanré, J.P. Buis, A. Setzer, E. Vermote, J.A.  
685 Reagan, Y.J. Kaufman, T. Nakajima, F. Lavenu, I. Jankowiak and A. Smirnov, 1998:  
686 AERONET--A federated instrument network and data archive for aerosol  
687 characterization. *Rem. Sens. Environ.*, **66**, 1-16.

688

689 Hsu, N. C., S. C. Tsay, M. D. King, and J. R. Herman, 2004: Aerosol properties over  
690 bright-reflecting source regions. *IEEE Trans. Geosci. Remote Sens.*, **42**, 557-569.

691

692 Ichoku, C., D.A. Chu, S. Mattoo, Y.J. Kaufman, L.A. Remer, D. Tanré, I. Slutsker and  
693 B.N. Holben, 2002: A spatio-temporal approach for global validation and analysis of  
694 MODIS aerosol products. *Geophys. Res. Lett.*, **29**, 10.1029/2001GL013206.

695

696 Ichoku, C., L. A. Remer, Y. J. Kaufman, R. Levy, D. A. Chu, D. Tanre, and B. N.  
697 Holben, 2003: MODIS observation of aerosols and estimation of aerosol radiative  
698 forcing over southern Africa during SAFARI 2000. *J. Geophys. Res.*, **108** (D13), 8499,  
699 doi: 10.1029/2002JD002366.

700

701 Ichoku, C., L. A. Remer, and T. F. Eck, 2005: Quantitative evaluation and  
702 intercomparison of morning and afternoon MODIS aerosol measurements from Terra  
703 and Aqua. *J. Geophys. Res.* **110**, D10S03, doi: 10.1029/2004JD004987.

704  
705 Jethva, H., S.K. Satheesh and J. Srinivasan, 2007: Assessment of second-generation  
706 MODIS aerosol retrieval (Collecton 005) at kanpur, India. *Geophys. Res. Lett.*, 34,  
707 L19802, doi:10.1029/2007GL029647.  
708  
709 Kaufman, Y. J., and C. Sende, 1988: Algorithm for atmospheric corrections of visible  
710 and Near IR satellite imagery. *Int. J. Rem. Sens.*, **9**, 1357-1381.  
711  
712 Kaufman, Y. J., D. Tanre, L. Remer, E. Vermote, A. Chu, and B. N. Holben, 1997:  
713 Operational remote sensing of tropospheric aerosol over land from EOS Moderate  
714 Resolution Imaging Spectroradiometer. *J. Geophys. Res. (Atmos.)*, **102**, 17051-17067.  
715  
716 Kaufman, Y. J., O. Boucher, D. Tanre, M. Chin, L. A. Remer, and T. Takemura, 2005:  
717 Aerosol anthropogenic component estimated from satellite data. *Geophys. Res. Lett.* **32**,  
718 L17804, doi:10.1029/2005GL023125.  
719  
720 Kleidman, R.G., N.T. O'Neill, L.A. Remer, Y.J. Kaufman, T.F. Eck, D. Tanré, and B.N.  
721 Holben 2005: Comparison of moderate resolution Imaging spectroradiometer (MODIS)  
722 and aerosol robotic network (AERONET) remote-sensing retrievals of aerosol fine mode  
723 fraction over ocean. *J. Geophys. Res.*, **110** D22205, doi:10.1029/2005JD005760.  
724  
725 Koren, I., L. A. Remer, Y. J. Kaufman, Y. Rudich, and J. V. Martins, 2007: On the  
726 twilight zone between clouds and aerosols. *Geophys. Res. Lett.*, **34**, L08805,  
727 doi:10.1029/2007GL029253.  
728  
729 Levy, R.C., L.A. Remer, D. Tanré, Y.J. Kaufman, C. Ichoku, B.N. Holben, J.M.  
730 Livingston, P.B. Russell and H. Maring, 2003: Evaluation of the MODIS retrievals of  
731 dust aerosol over the ocean during PRIDE. *J. Geophys. Res.*, **108** (D14),  
732 10.1029/2002JD002460  
733  
734 Levy, R. C., L. A. Remer, J. V. Martins, Y. J. Kaufman, A. Plana-Fattori, J. Redemann,  
735 P. B. Russell, and B. Wenny, 2005: Evaluation of the MODIS aerosol retrievals over  
736 ocean and land during CLAMS. *J. Atmos. Sci.*, **62**, 974-992.  
737  
738 Levy, R. C., L. A. Remer, and O. Dubovik, 2007: Global aerosol optical properties and  
739 application to MODIS aerosol retrieval over land . *J. Geophys. Res.*, **112**, D13210,  
740 doi:10.1029/2006JD007815.  
741  
742 Levy, R. C., L. Remer, S. Mattoo, E. Vermote, and Y. J. Kaufman, 2007: Second-  
743 generation algorithm for retrieving aerosol properties over land from MODIS spectral  
744 reflectance. *J. Geophys. Res.*, **112**, D13211, doi:10.1029/2006JD007811.  
745  
746 Levy, R.C., V. Zubko, G. Leptoukh, A. Gopalan, L.A. Remer, S. Kinne, submitted: A  
747 critical look at MODIS estimates of global monthly aerosol optical depth. Submitted to  
748 *Geophys. Res. Lett.*  
749

750 Li, R.-R., Y.J. Kaufman, B.-C. Gao and C.O. Davis, 2003: Remote sensing of suspended  
751 sediments and shallow coastal waters. *IEEE TGARS*, **41**, 559-566.

752

753 Livingston, J. M., P. B. Russell, J. S. Reid, J. Redemann, B. Schmid, D. A. Allen, O.  
754 Torres, R. C. Levy, L. A. Remer, B. N. Holben, A. Smirnov, O. Dubovik, E. J. Welton,  
755 J. R. Campbell, J. Wang, and S. A. Christopher, 2003: Airborne Sun photometer  
756 measurements of aerosol optical depth and columnar water vapor during the Puerto Rico  
757 Dust Experiment and comparison with land, aircraft, and satellite measurements. *J. Geophys. Res.-Atmos.* **108** (D19).

758

759

760 Martins, J.V., D. Tanré, L.A. Remer, Y.J. Kaufman, S. Mattoo and R. Levy, 2002:  
761 MODIS Cloud screening for remote sensing of aerosol over oceans using spatial  
762 variability. *Geophys. Res. Lett.*, **29**, 10.1029/2001GL013252.

763 O'Neill, N.T., T.F.Eck, , A.Smirnov, B.N.Holben, and S.Thulasiraman, Spectral  
764 discrimination of coarse and fine mode optical depht, *J. Geophys. Res.*, **108**(D17), 4559,  
765 doi:10.1029/2002JD002975, 2003.

766

767 Redemann, J., B. Schmid, J. A. Eilers, R. Kahn, R. C. Levy, P. B. Russell, J. M.  
768 Livingston, P. V. Hobbs, W. L. Smith, and B. N. Holben, 2005: Suborbital  
769 measurements of spectral aerosol optical depth and its variability at subsatellite grid  
770 scales in support of CLAMS 2001. *J. Atmos. Sci.*, **62**, No. 4, 993-1007.

771

772 Redemann, J., Q. Zhang, B. Schmid, P. B. Russell, J. M. Livingston, H. Jonsson, and L.  
773 A. Remer, 2006: Assessment of MODIS-derived visible and near-IR aerosol optical  
774 properties and their spatial variability in the presence of mineral dust. *Geophys. Res. Lett.*,  
775 **33**, L18814, doi:10.1029/2006GL026626.

776

777 Remer, L.A., D. Tanré, Y.J. Kaufman, C. Ichoku, S. Mattoo, R. Levy, D.A. Chu, B.N.  
778 Holben, O. Dubovik, A. Smirnov, J.V. Martins, R.-R. Li and Z. Ahmad, 2002:  
779 Validation of MODIS aerosol retrieval over ocean. *Geophys. Res. Lett.*, **29**,  
780 10.1029/2001GL013204.

781

782 Remer, L. A., Y. J. Kaufman, D. Tanre, S. Mattoo, D. A. Chu, J. V. Martins, R. R. Li; C.  
783 Ichoku, R. C. Levy, R. G. Kleidman, T. F. Eck, E. Vermote, and B. N. Holben, 2005:  
784 The MODIS aerosol algorithm, products and validation. *J. Atmos. Sci.*, **62**, 947-973.

785

786 Remer, L. A., and Y. J. Kaufman, 2006: Aerosol direct radiative effect at the top of the  
787 atmosphere over cloud free ocean derived from four years of MODIS data. *Atmos.*  
788 *Chem. & Phys.* **6**, 237-253.

789

790 Remer, L.A., D. Tanré, Y.J. Kaufman, R.C. Levy, S. Mattoo, 2006: Algorithm for  
791 Remote Sensing of Tropospheric Aerosol from MODIS: Collection 005. Algorithm  
792 Theoretical Basis Document available at [http://modis-atmos.gsfc.nasa.gov/reference\\_atbd.php](http://modis-atmos.gsfc.nasa.gov/reference_atbd.php).

793

794

795 Russell, P. B., J. M. Livingston, J. Redemann, B. Schmid, S. A. Ramirez, J. Eilers, R.  
796 Khan, D. A. Chu, L. Remer, P. K. Quinn, M. J. Rood, and W. Wang, 2007: Multi-grid-  
797 cell validation of satellite aerosol property retrievals in INTEX/ITCT/ICARTT 2004. *J.*  
798 *Geophys. Res.*, **112**, D12S09, doi: 10.1029/2006JD007606.  
799

800 Smirnov A., B.N.Holben, T.F.Eck, O.Dubovik, and I.Slutsker, 2000: Cloud screening  
801 and quality control algorithms for the AERONET database, *Rem.Sens.Env.*, **73**, 337-349.  
802 Tanre, D., M. Herman, and Y. Kaufman, 1996: Information on the aerosol size  
803 distribution contained in the solar reflected spectral radiances. *J. Geophys. Res.*, **101**,  
804 19043-19060.  
805

806 Tanre, D., Y. J. Kaufman, M. Herman, and S. Mattoo, 1997: Remote sensing of aerosol  
807 properties over oceans using the MODIS/EOS spectral radiances. *J. Geophys. Res.*  
808 (*Atmos.*), **102**, 16971-16988.  
809

810 Tanre, D., L. A. Remer, Y. J. Kaufman, S. Mattoo, P. V. Hobbs, J. M. Livingston, P. B.  
811 Russell, and A. Smirnov, 1999: Retrieval of aerosol optical thickness and size  
812 distribution over ocean from the MODIS Airborne Simulator during TARFOX. *J.*  
813 *Geophys. Res.*, **104**, 2261-2278.  
814

815 Wen, G., A. Marshak, and R. F. Cahalan, 2006: Impact of 3D Clouds on Clear Sky  
816 Reflectance and Aerosol Retrieval in a Biomass Burning Region of Brazil. *IEEE Geo.*  
817 *Rem. Sens. Lett.*, **3**, 169-172.  
818

819 Wen, G., A. Marshak, R. F. Cahalan, L. A. Remer, and R. G. Kleidman, 2007: 3D  
820 aerosol-cloud radiative interaction observed in collocated MODIS and ASTER images  
821 of cumulus cloud fields. *J. Geophys. Res.*, **112**, D13204, doi 10.1029/2006JD008267.  
822

823 Zhang, J., J.S. Reid, and B.N. Holben, 2005: An analysis of potential cloud artifacts in  
824 MODIS over ocean aerosol thickness products. *Geophys. Res. Lett.*, **32**, L15803,  
825 doi:10.1029/2005GL023254.  
826

827

828 **Figure Captions**

829

830 Figure 1. MODIS aerosol optical depth (AOD) over oceans plotted against collocated  
831 AERONET observations. Top: AOD at 550 nm. Bottom: AOD at 870 nm. Left:  
832 Collocations with the Terra satellite. Right: Collocations with the Aqua satellite. The  
833 data were sorted according to AERONET AOD, divided into 25 bins of equal  
834 observations, and statistics calculated. Points represent the means of each bin. Error bars  
835 represent the standard deviation of MODIS AOD within those bins. Highest AOD bin  
836 typically represents the mean of fewer observations than the other bins. AERONET  
837 AOD at 550 nm was interpolated on a log-log plot between observations at 500 nm and

838 675 nm. Stations with no 500 nm channel were not included in the upper plots, but were  
839 included in the lower plots where no interpolation was necessary. The regression line,  
840 regression equation and correlation were calculated from the full cloud of points before  
841 binning. Expected uncertainty is  $\pm 0.03 \pm 0.05 * \text{AOD}$ , and is shown in the plots by the  
842 dashed lines.

843

844 Figure 2 Similar as Figure 1, but for collocations over land. Only AOD at 550 nm is  
845 shown. Expected uncertainty over land is  $\pm 0.05 \pm 0.15 * \text{AOD}$ .

846

847 Figure 3. Histogram of aerosol optical depth at 550 nm (AOD) over ocean and fine mode  
848 fraction (FMF) derived from MODIS aerosol algorithms applied to a test bed of saved  
849 Collection 4 radiances. The test bed consisted of 35 granules of various oceanic aerosol  
850 scenes spread throughout 2001. Over 400,000 retrievals were used to construct the  
851 histograms. The Collection 4 results are shown in blue. Results of applying Collection 5  
852 software to Collection 4 radiances are shown in black. Solid curves denote AOD, and  
853 dotted curves denote FMF.

854

855 Figure 4. Global and monthly mean aerosol optical depth (AOD) at 550 nm over the  
856 global oceans from operational Collection 5 processing plotted against similar produced  
857 from old Collection 4 processing. Collection 5 processing includes both updates to the  
858 aerosol algorithm and also updates to the calibration. Terra and Aqua are plotted  
859 separately. Terra Collection 5 is higher than Terra Collection 4, and also higher than  
860 both Aquas.

861

862 Figure 5 Time series of MODIS global aerosol optical depth at 550 nm over ocean (left)  
863 and over land (right) for the length of the Aqua mission. Monthly mean total AOD is  
864 plotted with a heavy black line. Contribution to the AOD from fine mode (ocean) or fine  
865 model (land) is plotted in blue. Note that unlike ocean the land fine model contains  
866 coarse mode aerosols, as well. The percentile AODs are plotted by various dotted and  
867 dashed thin black lines. The mean AOD roughly corresponds to the 66% percentile over

868 both ocean and land, showing that 66% of the monthly mean AOD values are less than  
869 the mean. Note that the vertical axes are different in the land and ocean plots.

870

871 Figure 6. Global aerosol optical depth histograms (AOD) over ocean (left) and land  
872 (right) constructed from pixel-weighted daily  $1^{\circ} \times 1^{\circ}$  latitude-longitude MODIS aerosol  
873 products. Top: Calculated from all available data. Bottom: Calculated only for those  
874 grid squares with greater than 80% cloud cover. Line with solid circles shows mean fine  
875 mode (ocean) or fine model (land) AOD in each total AOD bin. Line with open circles  
876 shows mean fine mode fraction (ocean) or fine model fraction (land) in each AOD bin.  
877 Fine mode/model fraction is the fine AOD divided by the total AOD. Note that fine  
878 AOD and fine mode/model fraction are not the same quantities in the land and ocean  
879 plots. Fine model over land includes a coarse mode.

880

881 Figure 7. Five year mean global distribution of aerosol optical depth (AOD) at 550 nm  
882 for four selected months: January, April, July and October. The averages were calculated  
883 from pixel-weighted daily  $1^{\circ} \times 1^{\circ}$  latitude-longitude MODIS aerosol products. Negative  
884 values in purple identify where AOD is so low that it cannot be distinguished from zero,  
885 Black indicates fill value where no retrieval was attempted. Retrievals are not attempted  
886 over snow, during polar night or over bright deserts.

887

888 Figure 8 The 13 ocean regions (top) and 14 land regions (bottom).

889

890 Figure 9. Time series of regional and monthly mean aerosol optical depth (AOD) at 550  
891 nm calculated from pixel-weighted daily  $1^{\circ} \times 1^{\circ}$  latitude-longitude MODIS aerosol  
892 products. Regions are defined in Figure 8.

893

894 Figure 10. Monthly and regional mean fine mode AOD over ocean plotted against  
895 monthly and regional mean total AOD for five selected ocean regions. Regression lines  
896 and correlations are calculated and displayed. Regions fall into two classes defined by  
897 the slope of this regression. Most regions have slopes in the 0.7 to 0.8 range, as  
898 demonstrated by Region 4 (Asian Pacific) and denoted by the green line. However,

899 Region 6 (Saharan Atlantic) has a slope of 0.32 and is denoted by the blue line. Region 7  
900 (North Indian Ocean) has a seasonal shift with the months of October through March  
901 following the green line and months April through September following the blue line.

902

903

904

904 Table 1. Aerosol models used in Collection 5 MODIS ocean retrievals.  
905

## 906 Small Particles

	$\lambda=0.47 \text{ to } 0.86 \mu\text{m}$	1.24 $\mu\text{m}$	1.64 $\mu\text{m}$	2.13 $\mu\text{m}$	rg	$\sigma$	reff	comments
1	1.45-0.0035i	1.45-0.0035i	1.43-0.01i	1.40-0.005i	0.07	0.40	0.10	Wet water soluble type
2	1.45-0.0035i	1.45-0.0035i	1.43-0.01i	1.40-0.005i	0.06	0.60	0.15	Wet water soluble type
3	1.40-0.0020i	1.40-0.0020i	1.39-0.005i	1.36-0.003i	0.08	0.60	0.20	Water soluble with humidity
4	1.40-0.0020i	1.40-0.0020i	1.39-0.005i	1.36-0.003i	0.10	0.60	0.25	Water soluble with humidity

907  
908

## Large Particles

	$\lambda=0.47 \text{ to } 0.86 \mu\text{m}$	1.24 $\mu\text{m}$	1.64 $\mu\text{m}$	2.13 $\mu\text{m}$	rg	$\sigma$	reff	comments
5	1.35-0.001i	1.35-0.001i	1.35-0.001i	1.35-0.001i	0.40	0.60	0.98	Wet sea salt type
6	1.35-0.001i	1.35-0.001i	1.35-0.001i	1.35-0.001i	0.60	0.60	1.48	Wet sea salt type
7	1.35-0.001i	1.35-0.001i	1.35-0.001i	1.35-0.001i	0.80	0.60	1.98	Wet sea salt type
8	1.53-0.003i (0.47) 1.53-0.001i (0.55) 1.53-0.000i (0.66) 1.53-0.000i (0.86)	1.46-0.000i	1.46-0.001i	1.46-0.000i	0.60	0.60	1.48	Dust like type
9	1.53-0.003i (0.47) 1.53-0.001i (0.55) 1.53-0.000i (0.66) 1.53-0.000i (0.86)	1.46-0.000i	1.46-0.001i	1.46-0.000i	0.50	0.80	2.50	Dust like type

909  
910  
911

911

912 Table 2 Seasonal and annual aerosol optical depth at 550 nm (AOD) and fine mode  
913 fraction (FMF) for each ocean region of Figure 8  
914

	MAM		JJA		SON		DJF		annual	
	AOT	FMF	AOT	FMF	AOT	FMF	AOT	FMF	AOT	FMF
1	0.20	0.53	0.13	0.62	0.11	0.44	0.13	0.33	0.14	0.49
2	0.17	0.52	0.15	0.62	0.11	0.44	0.12	0.36	0.14	0.49
3	0.20	0.60	0.19	0.65	0.15	0.58	0.15	0.48	0.17	0.58
4	0.32	0.60	0.22	0.65	0.16	0.58	0.18	0.50	0.22	0.59
5	0.14	0.45	0.11	0.42	0.10	0.47	0.11	0.46	0.12	0.45
6	0.23	0.40	0.26	0.39	0.16	0.45	0.17	0.44	0.20	0.42
7	0.26	0.44	0.43	0.38	0.22	0.53	0.23	0.59	0.28	0.47
8	0.18	0.48	0.12	0.47	0.12	0.54	0.15	0.50	0.14	0.50
9	0.09	0.40	0.09	0.39	0.10	0.35	0.10	0.33	0.10	0.37
10	0.11	0.46	0.12	0.47	0.13	0.49	0.12	0.42	0.12	0.46
11	0.10	0.46	0.14	0.48	0.14	0.48	0.11	0.37	0.12	0.44
12	0.09	0.45	0.10	0.43	0.14	0.51	0.11	0.37	0.11	0.44
13	0.10	0.30	0.09	0.28	0.13	0.42	0.13	0.47	0.11	0.39

915

916

917

918 Table 3. Seasonal and annual aerosol optical depth at 550 nm for each land region of  
919 Figure 8.  
920

	MAM	JJA	SON	DJF	annual
1 West N. Am.	0.17	0.16	0.09	0.10	0.13
2 East N. Am.	0.13	0.17	0.06	0.05	0.10
3 Central Am.	0.25	0.15	0.12	0.10	0.15
4 S. Amer.	0.07	0.11	0.22	0.12	0.13
5 N. Europe	0.18	0.15	0.10	0.10	0.13
6. Mediter. Basin	0.22	0.25	0.16	0.13	0.19
7. N. Africa	0.38	0.34	0.24	0.29	0.31
8. S. Africa	0.11	0.21	0.21	0.14	0.17
9. Siberia	0.22	0.15	0.08	0.08	0.13
10. India	0.36	0.42	0.29	0.29	0.34
11. East Asia	0.46	0.35	0.24	0.27	0.33
12. SE Asia	0.39	0.28	0.24	0.21	0.28
13. Indonesia	0.17	0.19	0.28	0.19	0.21
14. Australia	0.03	0.01	0.07	0.07	0.04

921

922

923

923

924

925 Table 4. Annual mean aerosol optical depth at 550 nm (AOD), fine mode AOD, fine  
926 mode fraction (FMF), Angstrom Exponent defined by 550 nm and 870 nm, slope of the regression between AOD fine and AOD, and correlation of the regression.

Region	AOD	AOD fine	FMF	Ang1	slope	R <sup>2</sup>
1	0.14	0.07	0.49	0.65	0.72	0.79
2	0.14	0.07	0.49	0.66	0.81	0.80
3	0.17	0.1	0.58	0.87	0.69	0.77
4	0.22	0.13	0.59	0.84	0.71	0.94
5	0.12	0.05	0.45	0.60	0.49	0.83
6	0.20	0.09	0.42	0.52	0.32	0.90
7	0.28	0.13	0.47	0.65	0.22	0.58
8	0.14	0.07	0.50	0.67	0.57	0.84
9	0.10	0.04	0.37	0.45	0.30	0.40
10	0.12	0.06	0.46	0.60	0.64	0.81
11	0.12	0.06	0.44	0.59	0.70	0.88
12	0.11	0.05	0.44	0.59	0.65	0.83
13	0.11	0.04	0.39	0.44	0.76	0.91

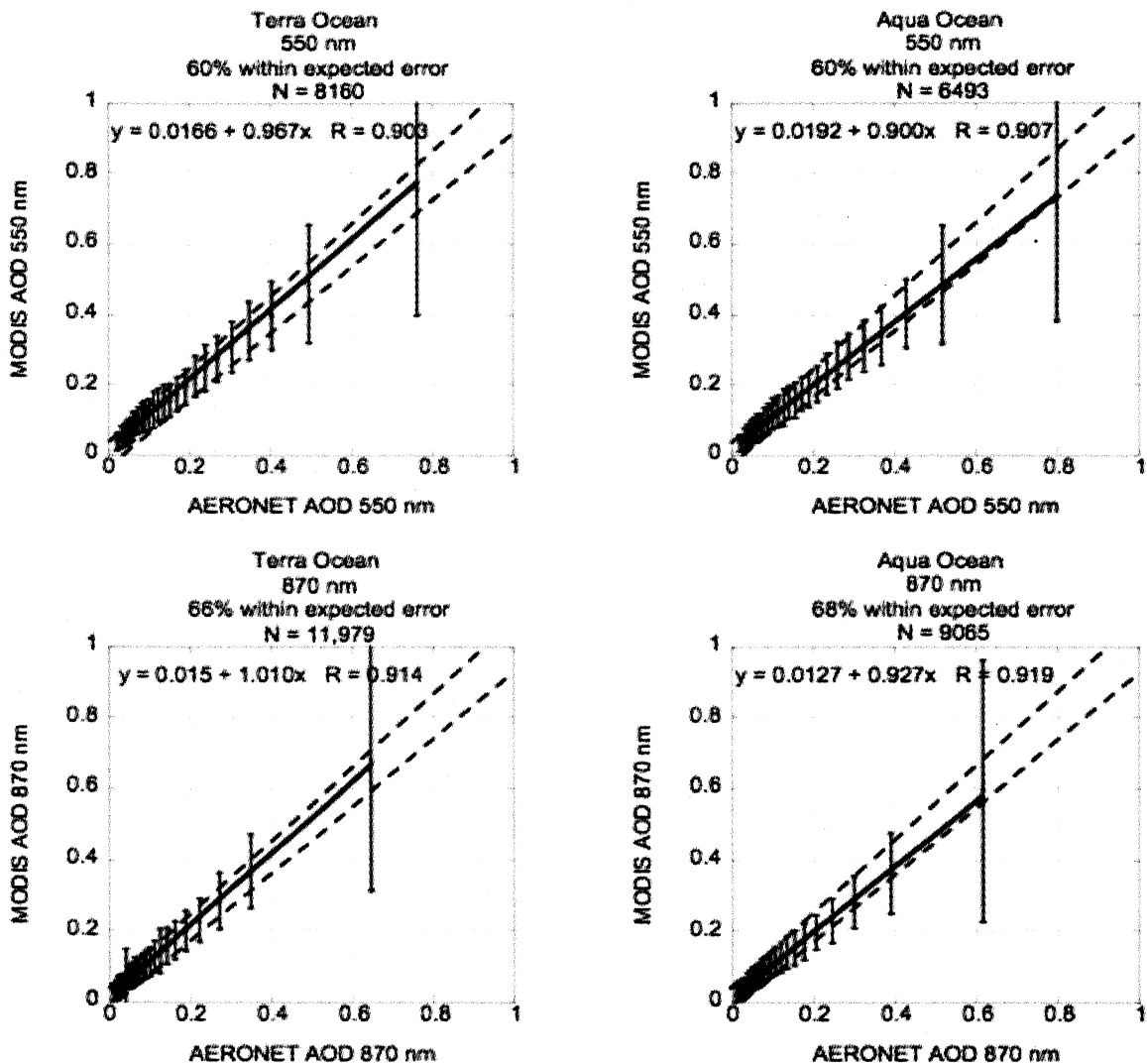
927

928

929

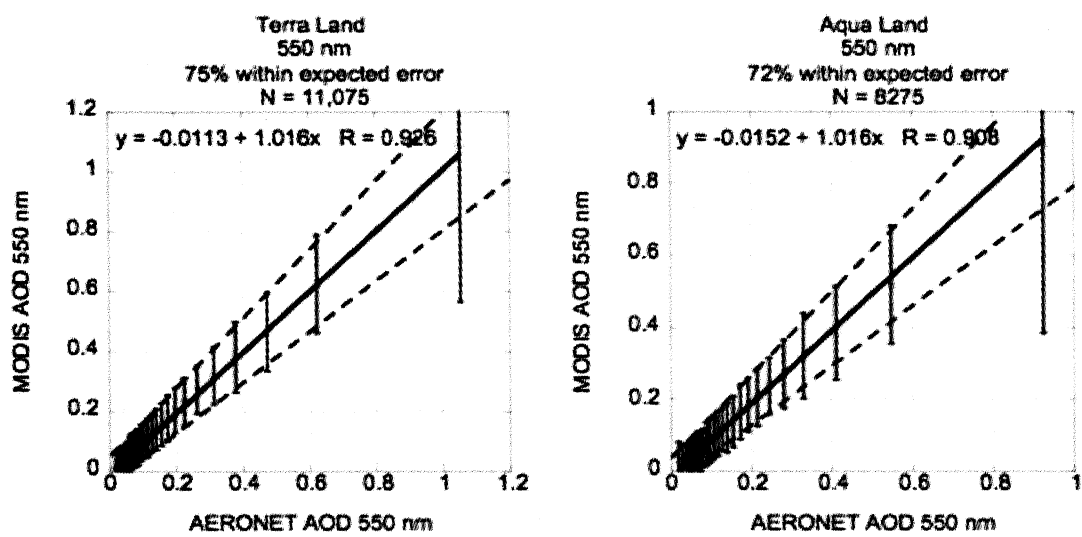
930

931



934 Figure 1. MODIS aerosol optical depth (AOD) over oceans plotted against collocated  
 935 AERONET observations. Top: AOD at 550 nm. Bottom: AOD at 870 nm. Left:  
 936 Collocations with the Terra satellite. Right: Collocations with the Aqua satellite. The  
 937 data were sorted according to AERONET AOD, divided into 25 bins of equal  
 938 observations, and statistics calculated. Points represent the means of each bin. Error bars  
 939 represent the standard deviation of MODIS AOD within those bins. Highest AOD bin  
 940 typically represents the mean of fewer observations than the other bins. AERONET  
 941 AOD at 550 nm was interpolated on a log-log plot between observations at 500 nm and  
 942 675 nm. Stations with no 500 nm channel were not included in the upper plots, but were  
 943 included in the lower plots where no interpolation was necessary. The regression line,  
 944 regression equation and correlation were calculated from the full cloud of points before  
 945 binning. Expected uncertainty is  $\pm 0.03 \pm 0.05 * \text{AOD}$ , and is shown in the plots by the  
 946 dashed lines.  
 947

947



948

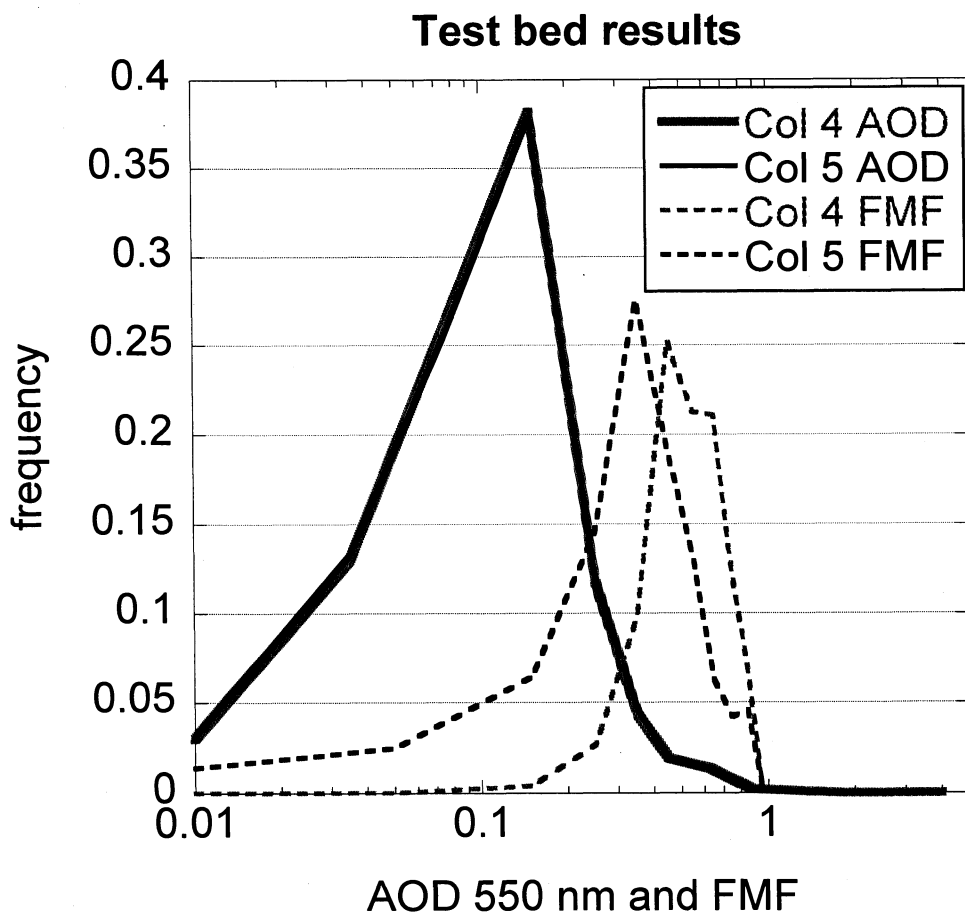
949

950 Figure 2 Similar as Figure 1, but for collocations over land. Only AOD at 550 nm is  
951      shown. Expected uncertainty over land is  $\pm 0.05 \pm 0.15 \times \text{AOD}$ .

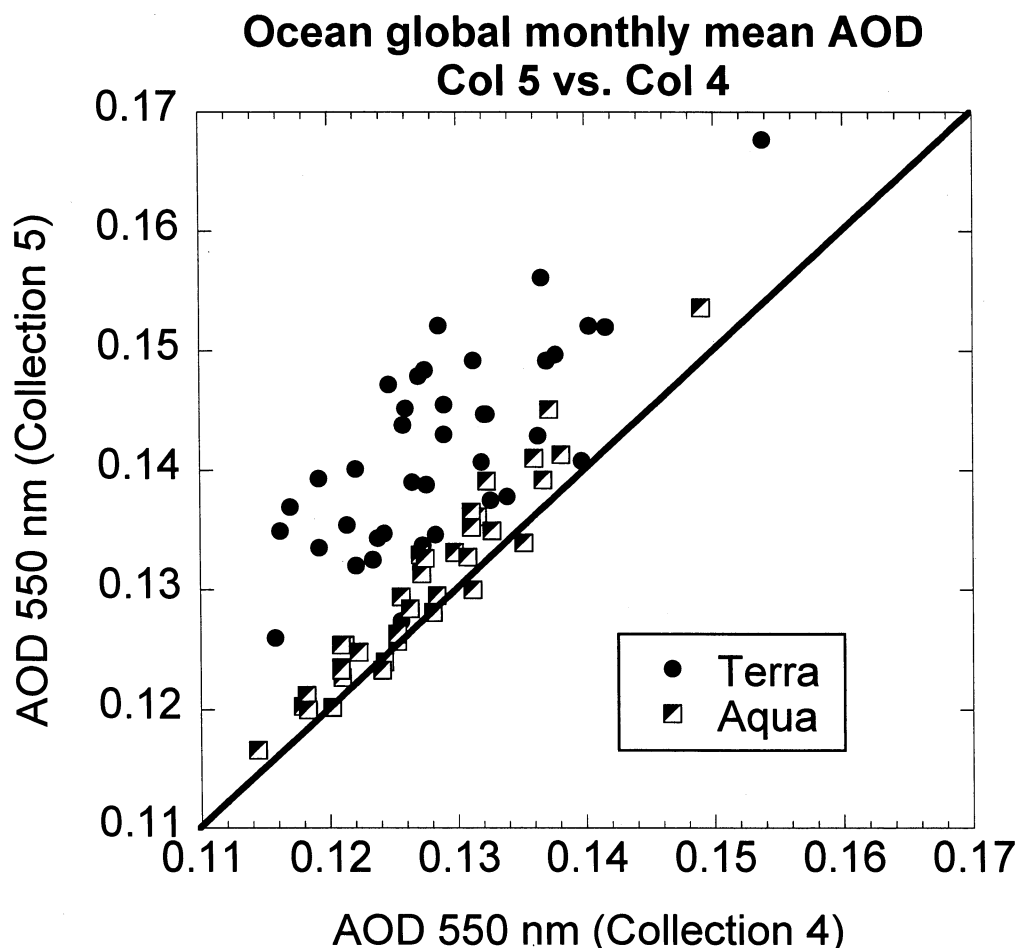
952

953

954

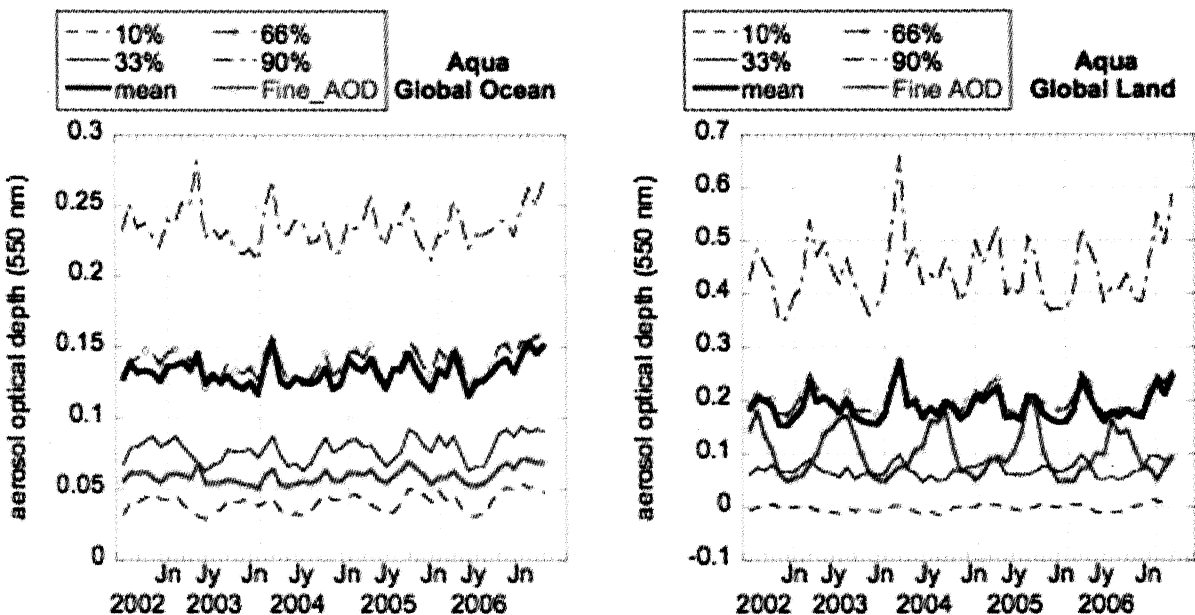


955      Figure 3. Histogram of aerosol optical depth at 550 nm (AOD) over ocean and fine mode  
 956      fraction (FMF) derived from MODIS aerosol algorithms applied to a test bed of saved  
 957      Collection 4 radiances. The test bed consisted of 35 granules of various oceanic aerosol  
 958      scenes spread throughout 2001. Over 400,000 retrievals were used to construct the  
 959      histograms. The Collection 4 results are shown in blue. Results of applying Collection 5  
 960      software to Collection 4 radiances are shown in black. Solid curves denote AOD, and  
 961      dotted curves denote FMF.  
 962  
 963

964  
965

966     Figure 4. Global and monthly mean aerosol optical depth (AOD) at 550 nm over the  
967     global oceans from operational Collection 5 processing, plotted against similar produced  
968     from old Collection 4 processing. Collection 5 processing includes both updates to the  
969     aerosol algorithm and also updates to the calibration. Terra and Aqua are plotted  
970     separately. Terra Collection 5 is higher than Terra Collection 4, and also higher than  
971     both Aquas.

972  
973  
974  
975  
976



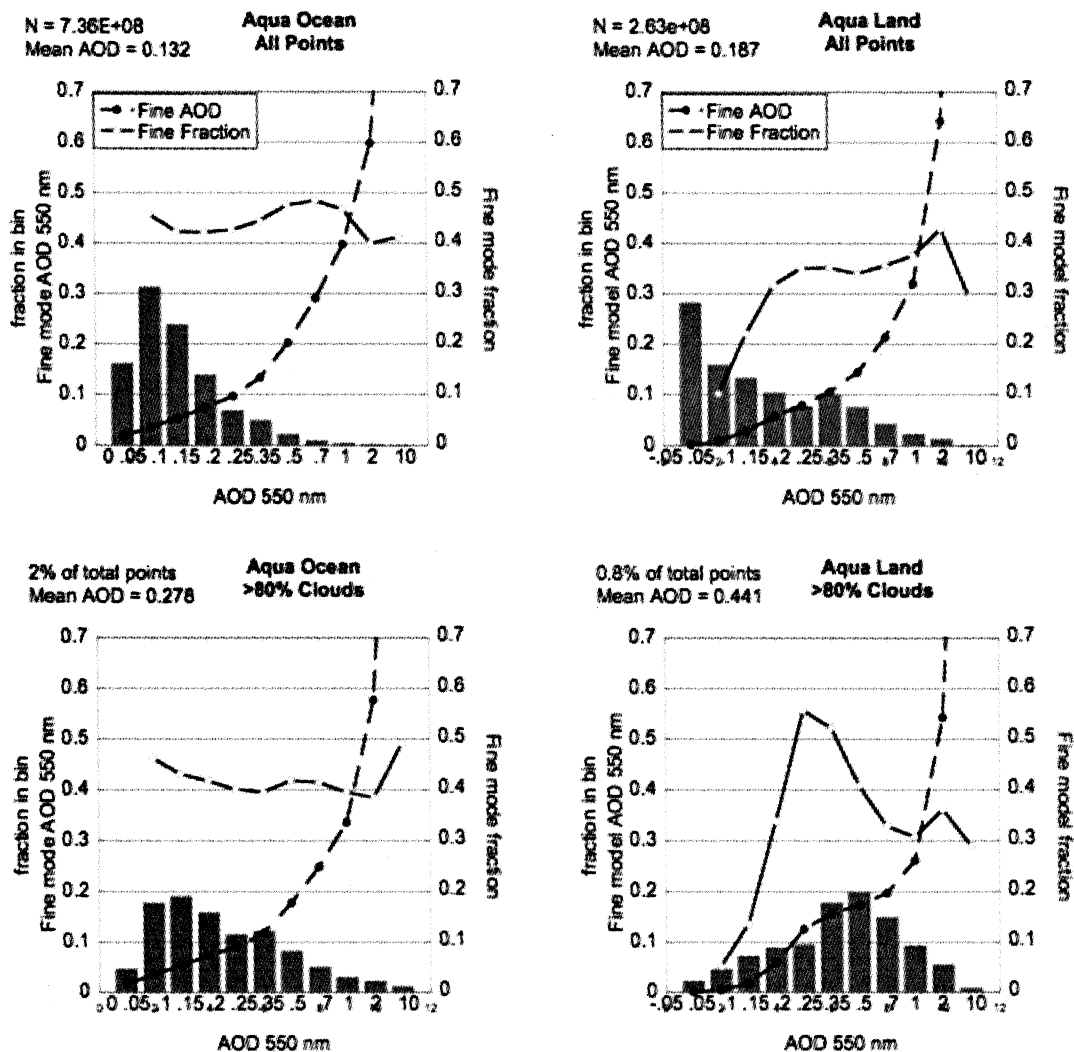
977

978

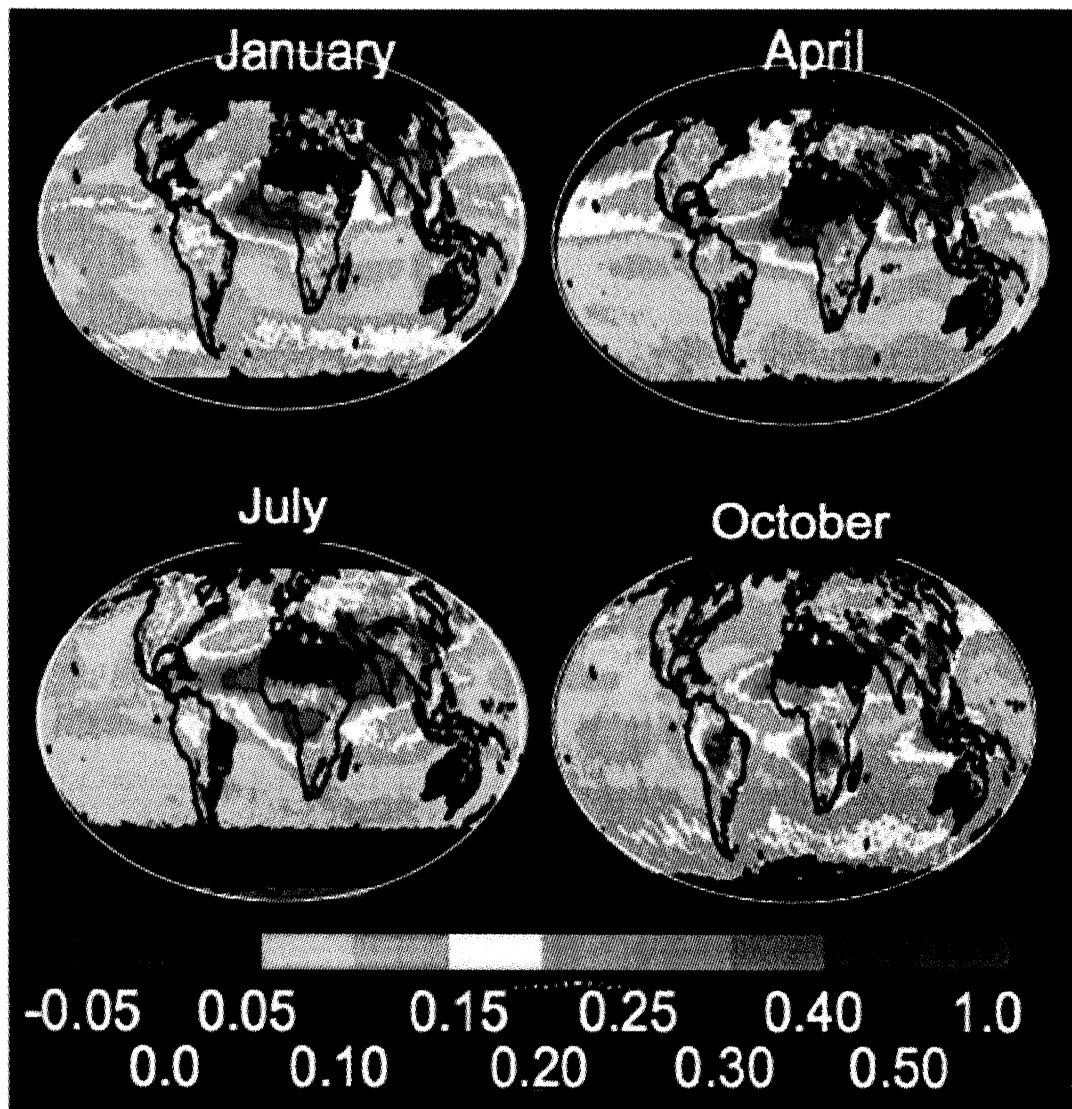
979 Figure 5 Time series of MODIS global aerosol optical depth at 550 nm over ocean (left)  
 980 and over land (right) for the length of the Aqua mission. Monthly mean total AOD is  
 981 plotted with a heavy black line. Contribution to the AOD from fine mode (ocean) or fine  
 982 model (land) is plotted in blue. Note that unlike ocean the land fine model contains  
 983 coarse mode aerosols, as well. The percentile AODs are plotted by various dotted and  
 984 dashed thin black lines. The mean AOD roughly corresponds to the 66% percentile over  
 985 both ocean and land, showing that 66% of the monthly mean AOD values are less than  
 986 the mean. Note that the vertical axes are different in the land and ocean plots.  
 987

988

989



992      Figure 6. Global aerosol optical depth histograms (AOD) over ocean (left) and land  
 993      (right) constructed from pixel-weighted daily  $1^{\circ} \times 1^{\circ}$  latitude-longitude MODIS aerosol  
 994      products. Top: Calculated from all available data. Bottom: Calculated only for those  
 995      grid squares with greater than 80% cloud cover. Line with solid circles shows mean fine  
 996      mode (ocean) or fine model (land) AOD in each total AOD bin. Line with open circles  
 997      shows mean fine mode fraction (ocean) or fine model fraction (land) in each AOD bin.  
 998      Fine mode/model fraction is the fine AOD divided by the total AOD. Note that fine  
 999      AOD and fine mode/model fraction are not the same quantities in the land and ocean  
 1000     plots. Fine model over land includes a coarse mode.



1003

1004

1005      Figure 7. Five year mean global distribution of aerosol optical depth (AOD) at 550 nm  
1006      for four selected months: January, April, July and October. The averages were calculated  
1007      from pixel-weighted daily  $1^{\circ} \times 1^{\circ}$  latitude-longitude MODIS aerosol products. Negative  
1008      values in purple identify where AOD is so low that it cannot be distinguished from zero,  
1009      Black indicates fill value where no retrieval was attempted. Retrievals are not attempted  
1010      over snow, during polar night or over bright deserts.

1011

1012

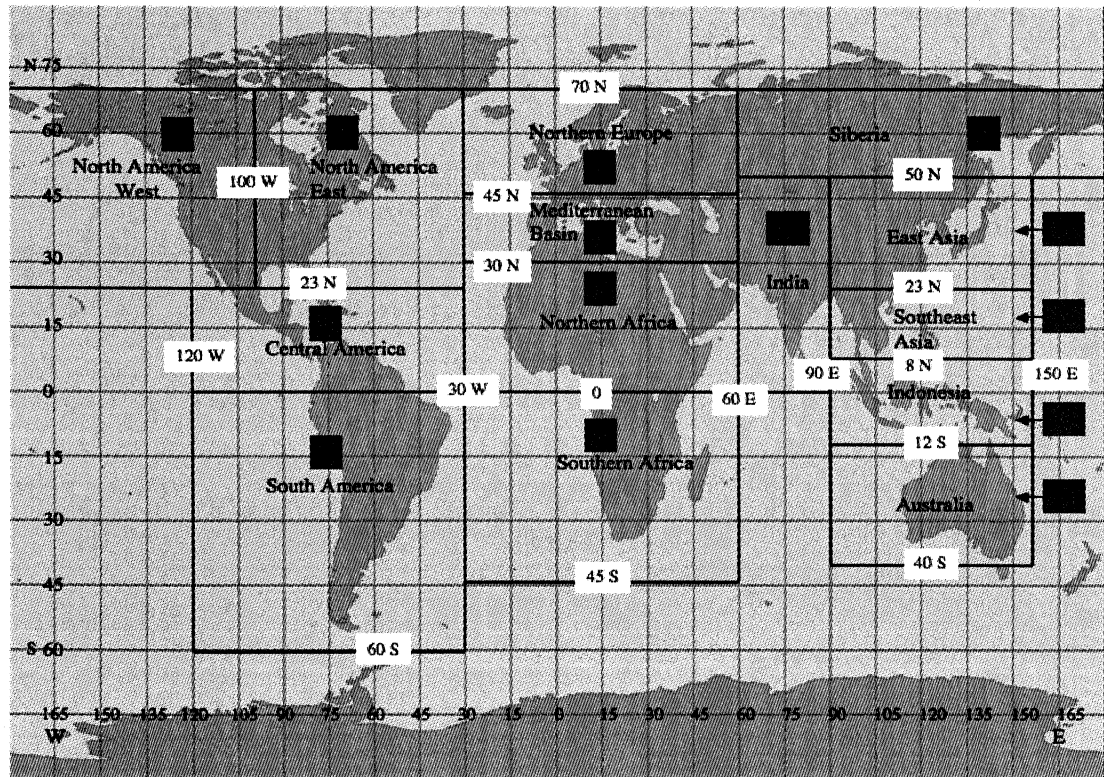
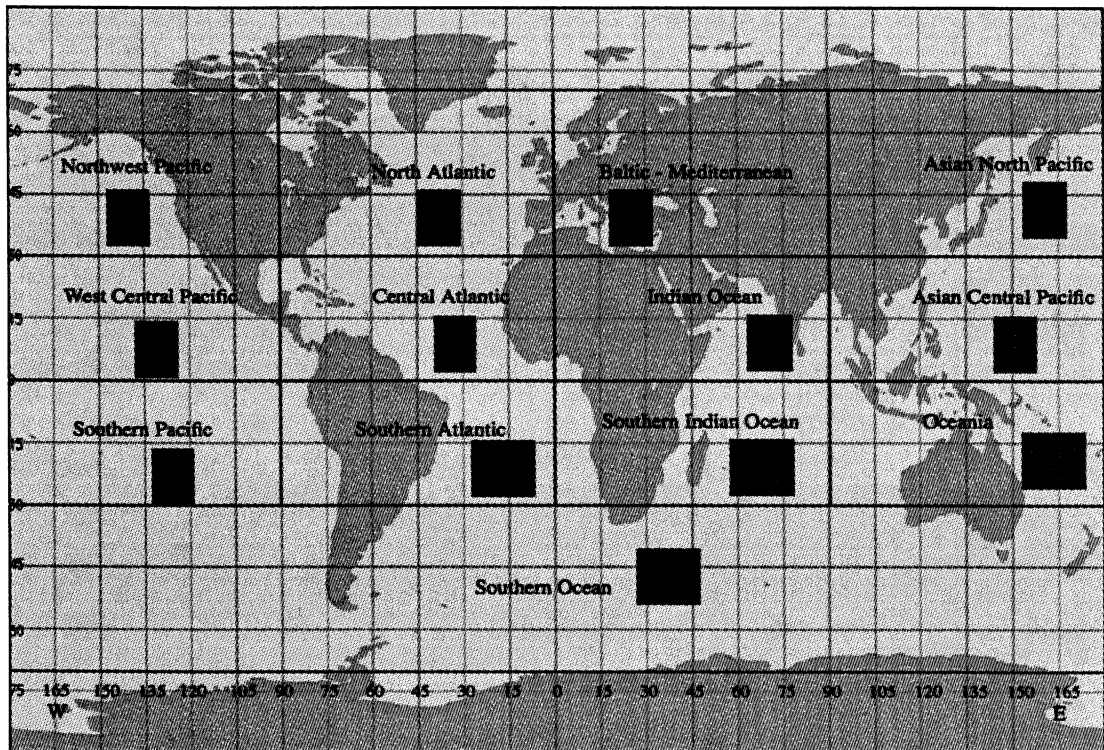
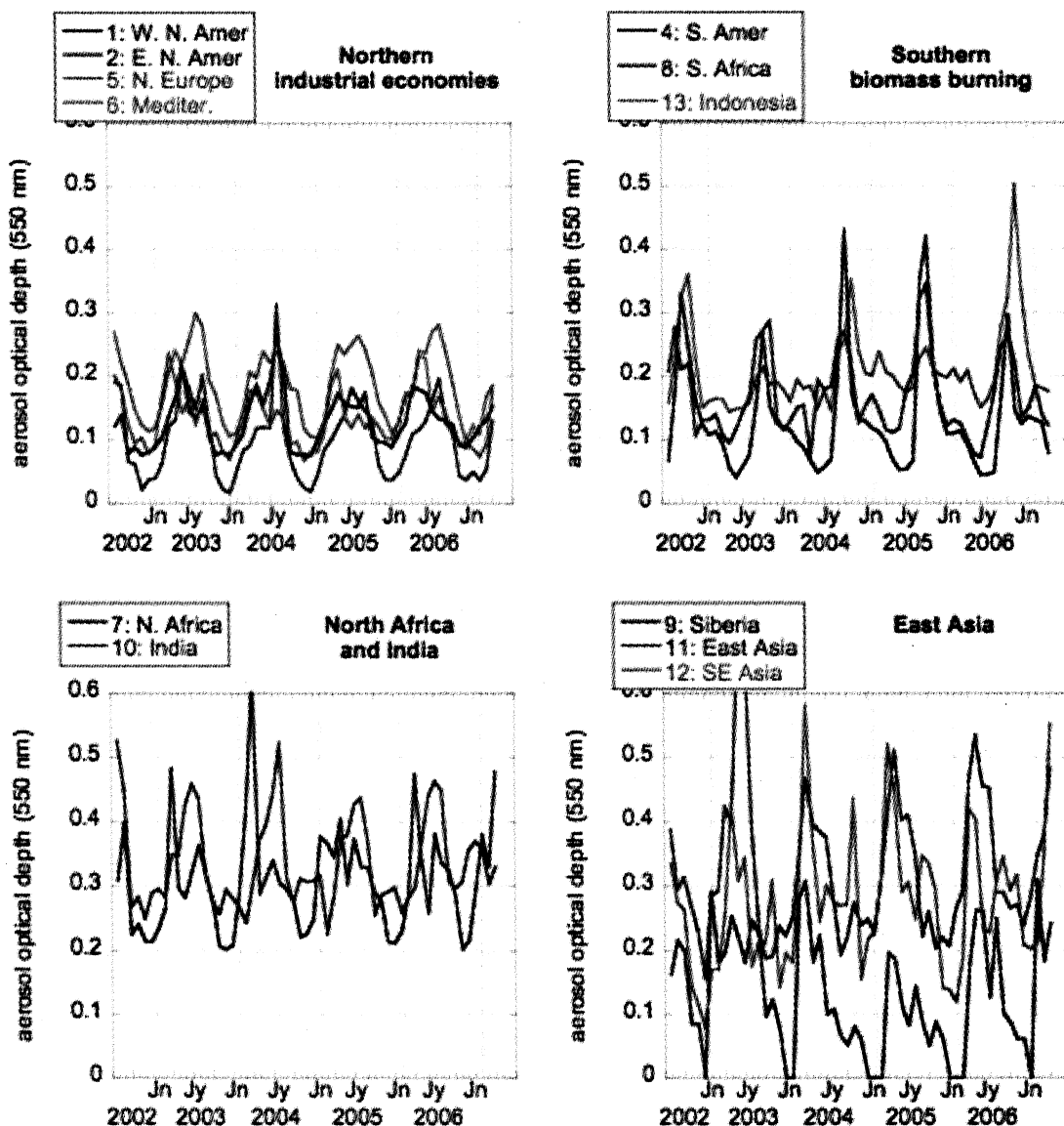
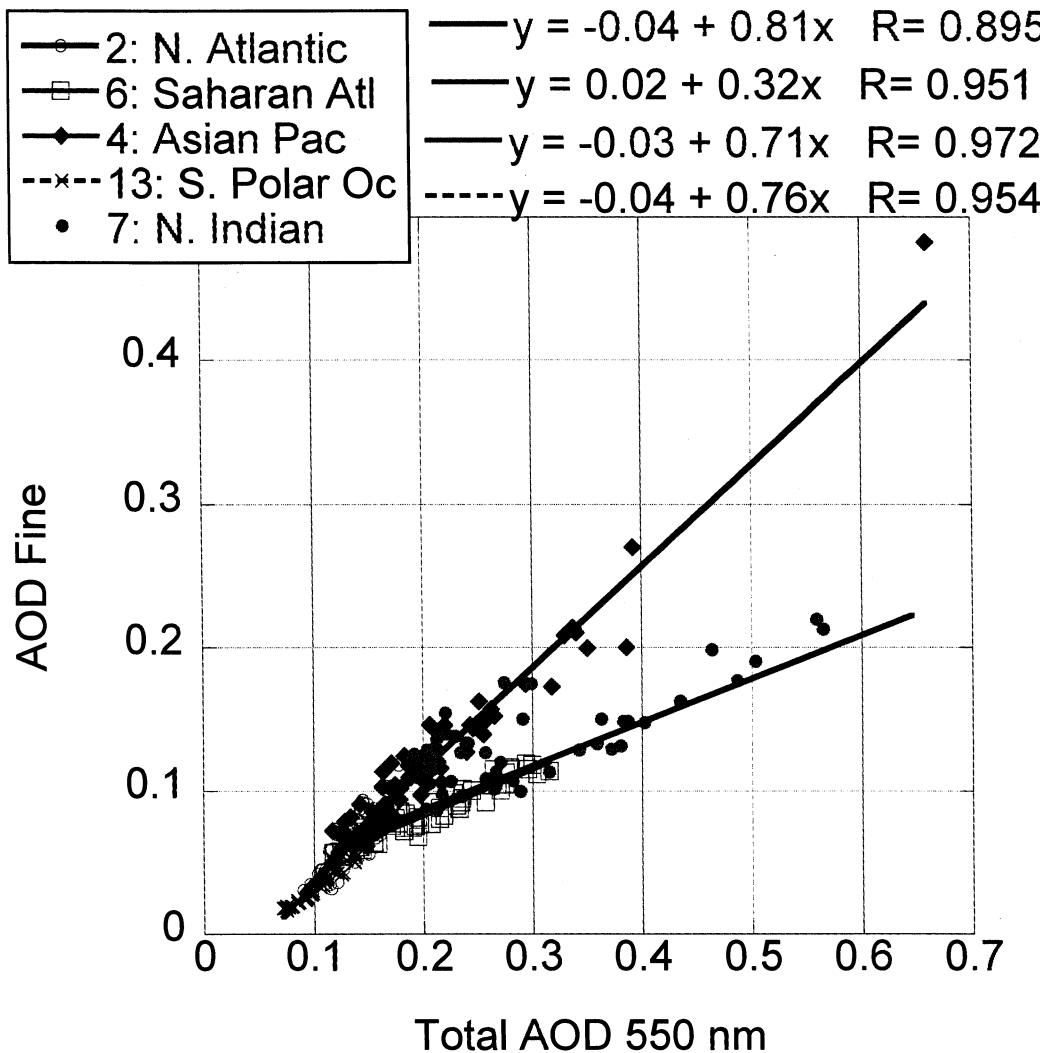


Figure 8 The 13 ocean regions (top) and 14 land regions (bottom).

1019  
1020



1021  
1022  
1023 Figure 9. Time series of regional and monthly mean aerosol optical depth (AOD) at 550  
1024 nm calculated from pixel-weighted daily  $1^{\circ} \times 1^{\circ}$  latitude-longitude MODIS aerosol  
1025 products. Regions are defined in Figure 8.  
1026  
1027



1028  
1029

1030 Figure 10. Monthly and regional mean fine mode AOD over ocean plotted against  
 1031 monthly and regional mean total AOD for five selected ocean regions. Regression lines  
 1032 and correlations are calculated and displayed. Regions fall into two classes defined by  
 1033 the slope of this regression. Most regions have slopes in the 0.7 to 0.8 range, as  
 1034 demonstrated by Region 4 (Asian Pacific) and denoted by the green line. However,  
 1035 Region 6 (Saharan Atlantic) has a slope of 0.32 and is denoted by the blue line. Region 7  
 1036 (North Indian Ocean) has a seasonal shift with the months of October through March  
 1037 following the green line and months April through September following the blue line.